Journal of Colloid and Interface Science 683 (2025) 1135–1149

Contents lists available at ScienceDirect

Journal of Colloid And Interface Science

journal homepage: www.elsevier.com/locate/jcis

Dynamic self-assembled *meso*-structures formed across a wide concentration range in aqueous solutions of propranolol hydrochloride

Yixuan Yan [a,*], Yichun Shen [a], Najet Mahmoudi [b], Peixun Li [c], James Tellam [c], Richard A. Campbell [a], David J. Barlow [a], Katharina Edkins [a,d], Andrew G. Leach [a], M.Jayne Lawrence [a]

[a] School of Health Sciences, Stopford Building, The University of Manchester, Oxford Road, Manchester M13 9PT, UK
[b] ISIS Pulsed Neutron and Muon Source, Rutherford Appleton Laboratory, Chilton, Didcot OX11 0QX, UK
[c] Deuteration Facility, ISIS Pulsed Neutron and Muon Source, Rutherford Appleton Laboratory, STFC, Chilton, Didcot OX11 0QX, UK
[d] Institute of Pharmacy and Biomedical Sciences, Strathclyde University, 161 Cathedral Street, Glasgow G4 0RE, UK

HIGHLIGHTS

- Propranolol hydrochloride self-associates in aqueous solution.
- A continuum of particle sizes is shown to exist across a wide concentration range.
- MD studies show that molecules join and leave aggregates on a nanosecond timescale.
- The aggregates are prolate ellipsoids with a polar shell and apolar core.
- Formation of the aggregates is driven by π-π or CH-π interactions.

GRAPHICAL ABSTRACT

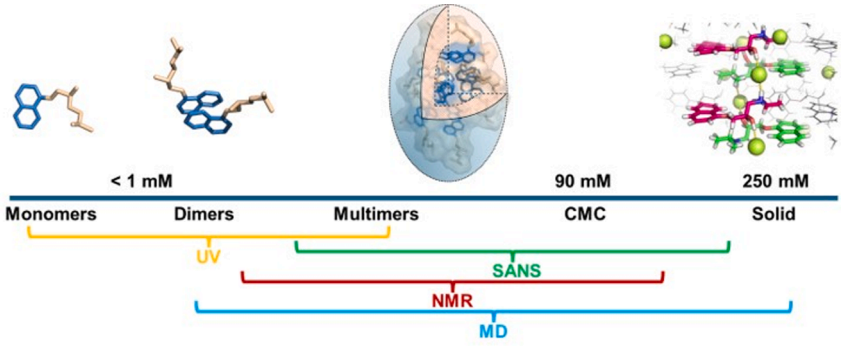

ARTICLE INFO

Keywords:
Colloidal systems
Small angle neutron scattering
Molecular dynamics
Nuclear magnetic resonance
Quantum mechanics
Drug self-association
Propranolol hydrochloride

ABSTRACT

Hypothesis: Nanoscale characterisation of the self-associated species formed by amphiphilic pharmaceuticals in aqueous solution carries relevance across their entire journey from development through to manufacture – relevant, therefore, not only as regards formulation of the drug products as medicines, but also potentially relevant to their bioavailability, activity, and clinical side effects. Such knowledge and understanding, however, can only be fully secured by applying a range of experimental and theoretical methodologies.
Experiments: Herein, we apply a synergistic combination of solubility, surface tension, SANS, NMR and UV spectroscopic studies, together with MD simulation and QM calculations, to investigate the *meso*-structures of propranolol hydrochloride aggregates in bulk aqueous solutions, at concentrations spanning 2.5 mM to > 200 mM. In addition, we explore the effects of adding NaCl to mimic the ionic strength of physiological fluids, and the differences between racemate and single enantiomer.
Findings: There is a continuum of particle sizes shown to exist across the *entire* concentration range, with molecules joining and leaving on the nanosecond timescale, and with the distributions of aggregate sizes varying with drug and salt concentration. Given that propranolol is a highly prescribed (WHO essential) medicine,

* Corresponding author at: School of Health Sciences, Stopford Building, The University of Manchester, Oxford Road, Manchester M13 9PT, UK.
E-mail address: yixuan.yan@manchester.ac.uk (Y. Yan).

https://doi.org/10.1016/j.jcis.2024.12.131
Received 2 October 2024; Received in revised form 16 December 2024; Accepted 17 December 2024
Available online 18 December 2024

disfavouring aggregators from consideration in high-throughput screening for potential new drug candidates – as many have advocated – should thus be done cautiously.

1. Introduction

Nanoscale characterisation of the self-associated species formed by amphiphilic pharmaceuticals in aqueous solution carries relevance across their entire journey from development through to manufacture and use. Knowing the supramolecular architectures of the self-associated species and understanding the mechanism(s) of their formation, is relevant not only as regards formulation of the drug products as medicines, but also potentially relevant to their bioavailability, activity, and clinical side effects.

More widely, such knowledge will contribute too to our understanding of the molecular mechanism(s) leading to solute nucleation and crystallisation (*cf.*, [1]), and it will thus provide insight to guide the design of preparation protocols employed in chemicals manufacture, and pertinent, therefore, not just to pharmaceuticals, but also to dyes, agrochemicals, and food stuffs.

The first studies of the self-association of pharmaceuticals were focussed on the antipsychotic phenothiazines [2,3]. Experiments performed using a combination of NMR, conductivity, viscosity, and light scattering measurements showed that these drugs form micellar aggregates, with aggregation numbers of 8 – 12, and critical micelle concentrations (cmc) in the millimolar range. Subsequent research, as reviewed by Schreier *et al.* [4], showed that a great many other drugs show similar behaviour, this list including numerous examples of local anaesthetics, analgesics, antibiotics, anti-histamines, and anti-hypertensive agents. As found for the phenothiazines, these drugs are shown to have cmc typically in the range 10 – 100 mM, with aggregation numbers of the order of 4 – 20.

For those drugs that possess anionic or cationic groups and exhibit poor aqueous solubility, it is common practice to use the device of salt formation as a means to improve drug solubilisation, but if the drug of interest also self-associates in solution, this will likely affect the pK_a of the ionisable group, and this in turn will lead to non-ideality of salt solubility (*cf.*, [5]) and might thus confound the formulation of the required solid dosage form. Moreover, Abramov *et al.* [6] have shown, by means of crystal growth morphology simulations, that the solution phase aggregation of self-associating drugs can adversely affect the kinetics of their crystallisation, so that crystals are not formed (as desired) with the drug in its thermodynamically most stable polymorphic form but with the drug instead crystallising as a metastable polymorph. If, over time, the metastable polymorph then transforms to the stable polymorph, either in the scale-up for manufacturing or over the course of the marketed product shelf-life, this might then compromise product performance and necessitate a costly reformulation – as proved necessary for GSK's Zantac, Abbott Laboratories' Norvir, and USB's Neupro (see, [7]).

There may be issues too that arise for liquid formulations, such as ophthalmic preparations, wherein the micelles formed by self-associating drugs might solubilise sparingly soluble additives in the preparations and might thereby reduce their physical and/or microbiological stability (*cf.*, [8]).

While the circulating concentrations of self-associating drugs required to achieve therapeutic effect will generally be significantly lower than their cmc, it is nevertheless likely that local concentrations of the drugs might exceed their cmc, and in this event, their self-association is likely to have adverse consequences on their rate of passage across membranes and into cells. Such a consequence was demonstrated by Khan *et al.* [9] who showed that self-association leads to a reduced cellular bioavailability of DNA minor groove-binding terbenzimidazoles. Likewise, Seelig *et al.* [10] showed a link between the cmc of self-associating drugs and their capacity to penetrate the blood–brain barrier, and Inacio *et al.* [11] showed that the kinetics of (passive) transport of tetracaine across both artificial membranes and pig skin showed significant variation as a function of the drug's aggregation state.

In addition, if the local concentration of a self-associating drug in the vicinity of a cell membrane rises sufficiently high, such that partitioning of the drug into the membrane leads to a locally high drug:lipid ratio, there is the further possibility that the drug might cause lipid flip-flop, solubilisation, or non-bilayer phase formation [12], and the resulting membrane disruption might then manifest as clinical side effects.

Many studies of the self-associated species present in solution resort to trapping molecules as a solid even though it may not be directly relevant to the solution state. This is a generally acknowledged limitation of techniques such as protein or small molecule crystallography [13] but is also the case for transmission electron microscopy studies [14–23], atomic force microscopy [16,22–25], or for the recently highlighted interferometric scattering microscopy that are interpreted as being directly relevant to the solution state [26].

Meanwhile, although giving data on interaction strengths and solution kinetics, structural interpretation remains challenging for time-averaged measurements made directly on the solution state such as those provided by dynamic (and static) light scattering [14–20,25,27–30], surface tension measurements [17,18,24], and variable concentration NMR spectroscopy [14,29–32]. Fluorimetry is only applicable to molecules that contain appropriate fluorophores and adding these features may significantly perturb the system [14,15,26].

Computational approaches can link these measurements back to molecular-scale structures [33–35]. Scattering experiments (performed using X-rays or neutrons), especially small angle scattering, provide a direct measurement of features on the time-scale of a collision but their interpretation often classifies solution features as regular shapes rather than in atomic detail [14,23,25,32,35,36]. The SASSIE suite of programs can help to make this link but applications so far are almost exclusively for proteins [37]. Simulations of structures that are consistent with experiment provide a means of interpreting these experiments [35,38].

We have focused here on experimental methods that directly interrogate the liquid state, without requiring the addition of fluorophores and have adopted a weight of evidence approach using relevant physical and computational techniques. We have measured the solubility and surface tension; have applied neutron scattering, NMR and UV spectroscopy; and have used quantum mechanics and molecular dynamics calculations. We have also considered previous dynamic light scattering, conductivity and NMR data [29,30,39].

With this powerful and complementary array of methods, we set out to study solutions of the beta-blocker propranolol (Fig. 1). This treatment for a range of cardiac health problems is one of the top 100 most prescribed medicines in the USA and UK and is used as a racemate [40,41]. It is most commonly used as a hydrochloride salt of the racemic mixture (**1**) and this is the form we have studied. The system was chosen because it was already known that it forms aggregates at high concentrations, and we wished to study the structure of these species. Unexpectedly, it was discovered that a continuum of particle sizes forms as concentration is changed. These vary from simple dimers to large, dynamic, liquid-like droplets containing tens of molecules; these heterogeneities are present in an apparently homogeneous solution and we have considered their structural relationship to pre-nucleation clusters in the crystallization pathway by comparing their structure to that in the solid state [42–44].

In addition to varying the concentration of **1**, the effect of adding NaCl to mimic the ionic strength of physiological fluids, and the contrast between racemate and a single enantiomer have also been investigated.

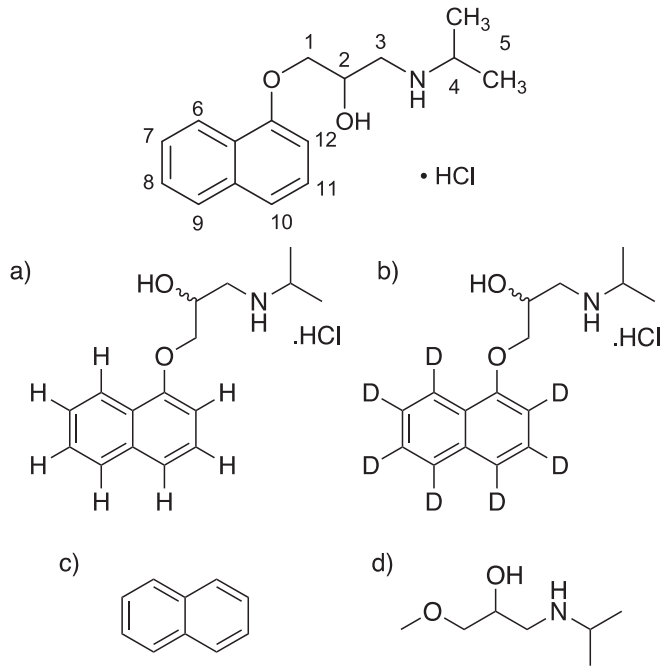

Fig. 1. Upper Panel: Propranolol hydrochloride (**1**) with protons numbered; Lower Panels: molecular structures of (a) protiated (*h*-**1**) and (b) deuterated (d_7-**1**) propranolol hydrochloride and the fragments (c): naphthalene ring and (d): 1-oxy-3-propan-2-ylamino)propan-2-ol side chain.

The observed structuring suggests that current models for understanding dynamic organization in solution that are based on continuum behaviour or that assume a small or non-existent polydispersity might not be generally applicable. Further, we find that the apparent critical aggregation concentration would seem not to correspond to the point at which aggregation *commences* but more likely indicates a change in the degree and/or the nature of the aggregation.

2. Materials & methods

2.1. Materials

(±)-Propranolol hydrochloride (99.9 %) and its isomers, (*S*)-(−)-propranolol hydrochloride and (*R*)-(+)-propranolol hydrochloride, were purchased from Alfa Aesar. Deuterium oxide (D_2O, 99.9 %-d), dichloromethane (DCM, ≥ 99.8 %), ethyl acetate (EtOAc, ≥ 99 %), diethyl ether (DEE ≥ 99 %) and sodium chloride (NaCl, 99.9 %) were obtained from Sigma Aldrich, while chloroform ($CHCl_3$ ≥ 99.8 %) was supplied by Fisher Scientific. Milli-Q (ultra-pure) water, with the resistivity of 18.2 MOhm cm, was obtained from a Suez pure water system.

2.2. Methods

2.2.1. Synthesis of d_7-propranolol hydrochloride

d_7-propranolol hydrochloride was synthesised by a three-step procedure. In the first reaction, the side chain was added to fully deuterated naphthol (2,3,4,5,6,7,8-heptadeuterio-1-napthol) via the Williamson ether synthesis using 2-(chloromethyl)oxirane. The product of this reaction, 2-[(2,3,4,5,6,7,8-heptadeuterio-1-naphthyl)oxymethyl]oxirane, was reacted with isopropylamine to add an isopropylamine group to the terminal oxirane moiety thereby preparing d_7-propranolol. Finally, the free base was acidified to prepare the required d_7-propranolol hydrochloride. Full details on the synthesis and characterisation are given in the Supplementary Information.

2.2.2. UV spectroscopy of propranolol hydrochloride

The UV spectra of **1** in H_2O were measured at room temperature in a 10 mm path length cell over the wavelength range from 200 to 350 nm, at a resolution of 1 nm, using a PerkinElmer Lambda 365 UV/VIS Spectrometer (Waltham, USA). When comparing the effect of concentration, UV spectra at ten concentrations of **1** over the range 0.45 mM – 0.011 mM were measured and the data were normalised to an absorbance value of **1** at a wavelength of 214 nm.

2.2.3. NMR spectroscopy of propranolol hydrochloride

^{1}H NMR spectra (range −4 to 16 ppm at a resolution of 0.002 ppm) of **1** in D_2O, with and without NaCl, were measured at room temperature over the concentration range 2.5 mM – 180 mM using a Bruker Avance-III HD 500 spectrometer (Karlsruhe, Germany). DCM, chemical shift of 5.33 ppm, was used as external standard. Analysis of the NMR data was performed using MestreNova 14.2 (Mestrelab Research, Spain).

An iterative spin simulation using the algorithm implemented in TopSpin (Bruker, Karlsruhe, Germany) was performed on five key protons in the sidechain (those attached to C1, *C*2 and C3), in order to understand the shifts and coupling patterns (see Supplementary Information).

2.2.4. Aqueous solubility of propranolol hydrochloride

The solubilities of **1** in H_2O and D_2O, with and without 0.154 M NaCl were determined (in quadruplicate) at room temperature and at 310 ± 1 K. An excess of **1** was added to the required solvent contained in a microfuge tube which was then sealed, protected from light, and mechanically agitated on a rotating wheel for 10 days at the required temperature, after which time the samples were centrifuged at 1000 rpm (Beckman Microfuge 16, Beckman Coulter, High Wycombe, UK) for 5 min to sediment any excess drug. An aliquot (10 μL) of the resultant supernatant was diluted 2,000-fold using the appropriate aqueous solvent. The amount of **1** dissolved was established by measuring the UV absorbance of the solution at the wavelength of the maximum absorbance [45] at a resolution of 1 nm using a PerkinElmer Lambda 365 UV/VIS spectrometer (Waltham, USA).

2.2.5. Surface tension measurements

Surface tension measurements were performed using the Wilhelmy plate method (EzPi, Kibron, Helsinki, Finland) using an inert metal alloy as the plate, to determine the surface activity of **1** (either as purchased or specifically purified) in aqueous solution at room temperature. **1** (300 mM) was dissolved in ultrapure water (surface tension corresponding to 72.8 mN m^{-1} at 293.15 K) with the use of ultrasonics and its surface tension measured as a function of concentration. Surface tension was recorded every 15 s until it reached equilibrium, immediately subsequent to equilibrium, 10 further data points were collected and used to determine the average surface tension at each concentration of **1** tested. At concentrations of 150 – 300 mM of **1**, surface tension measurements took about 30 min to equilibrate, at concentrations around the cmc (50 – 150 mM) measurements took 1 h, while at concentrations of **1** of less than 50 mM measurements required only 20 min equilibration.

2.2.6. Contrast variation small angle neutron scattering

Small angle neutron scattering studies (SANS) on **1** in solution were performed on the SANS2D beamline at the ISIS Pulsed Neutron and Muon Source (ISIS, Rutherford-Appleton Laboratory, Didcot, UK). The scattering pattern of neutrons after their interaction with sample was recorded on 2 96.5 x 96.5cm^2 two-dimensional detectors at a distance of 2.4 and 4 m from the sample. As SANS2D utilizes neutrons with wavelengths in the range 1.75 Å − 16.5 Å, the geometry employed yielded a scattering vector, $Q = 4\pi\sin(\theta)/\lambda$ in the range 0.0045 $Å^{-1} \leq Q \leq 0.7$ $Å^{-1}$. All samples were measured in disc-shaped quartz cuvettes (Hellma UK Ltd) of 1 mm or 2 mm path length (depending upon the deuterium content of the solvent) using a 12 mm diameter neutron beam and measured at 298 ± 0.1 K. After correction of the SANS data due to

instrumental factors, the scattering intensity ($I(Q)$) of the sample was calculated as a function of scattering vector (Q) after subtraction of the scattering intensity due to the solvent. Scaling with scattering from a partially deuterated polystyrene standard allowed determination of the absolute scattering cross-section of the sample (in units of cm^{-1}), with an error of approximately ± 2 %.

Stock solutions of protiated and partially deuterated d_7-propranolol hydrochloride in H_2O (*h*- or d_7-propranolol hydrochloride/H_2O) and in D_2O (*h*- or d_7-propranolol hydrochloride/D_2O) were prepared and diluted with the appropriate aqueous solvent to form solutions of concentration in the range 110 – 200 mM. With the exception of 200 mM propranolol hydrochloride, where it was not possible to prepare deuterated d_7-propranolol hydrochloride in D_2O at room temperature due to the lower solubility of the partially deuterated form of the drug in D_2O, 4 isotopic contrasts of **1** were measured, namely *h*- or d_7-propranolol hydrochloride in H_2O and *h*- or d_7-propranolol hydrochloride in D_2O. At concentrations of **1** of 60, 70 and 90 mM, only 2 contrasts (namely *h*-propranolol hydrochloride/D_2O and d_7-propranolol hydrochloride/H_2O) were measured as the scattering from the other two contrasts was too low.

The SANS of *h*-propranolol hydrochloride in either D_2O or D_2O containing 0.154 mM NaCl were measured over a concentration range of 30–200 mM at 298 ± 0.1 K.

A series of freshly purified *h*-propranolol hydrochloride in D_2O solutions were prepared in order to determine whether there was any difference in the resultant scattering behaviour observed with the corresponding 'as purchased' samples.

Samples of (R)-(+)-propranolol hydrochloride and (S)-(−)-propranolol hydrochloride in D_2O were measured at concentrations of 150, 130 and 110 mM at 310 K. In all cases the samples were initially bath sonicated for at least 40 min to ensure clarity of the samples.

Scattering intensity is described in terms of a form factor, $P(Q)$, and a structure factor, $S(Q)$:

$$I(Q) \propto \frac{N}{V} \langle \Delta\rho \rangle^2 V_p^2 P(Q) S(Q)$$

where N is the number of particles; V is the total volume of the system and V_p is the volume of a particle; $\Delta\rho$ is the difference in scattering length density (SLD) of the particle and the solvent. The term $\frac{N}{V}\langle \Delta\rho \rangle^2 V_P^2$ can be used to calculate the molecular weight of the particle. In the present study, a variety of form factors [$P(Q)$] were investigated including triaxial ellipsoids of uniform scattering length density, and core–shell spherical, prolate, and oblate spheroids, together with structure factors [$S(Q)$] of the Hayter-Penfold (H—P) and hard sphere models for charged [46,47] and uncharged aggregates, respectively [48]. Model-fitting of the data was performed using the program SasView [49]. The 3 or 4 contrasts measured for each propranolol hydrochloride concentration were modelled simultaneously (over the Q range 0.02 $Å^{-1}$ to 0.6 $Å^{-1}$) using the SasView package to obtain the best fit to the data. When modelling the data, a number of parameters were fixed, namely the SLD of the solvent (H_2O or D_2O) and the SLD of the propranolol hydrochloride and, for the core–shell models, the SLD of the particle core. For the Hayter-Penfold $S(Q)$, the dielectric constant of the solvent and temperature were fixed. It should be noted that it did not prove possible to correct the SANS data in the present study for scattering due to the cmc as it was not possible to measure a concentration of propranolol hydrochloride low enough to detect only the presence of monomers. (Further details of the methodology employed in model-fitting the SANS data are given in Supplementary Information.)

It was established that the model that gave the best fit to the SANS data, regardless of the absence or presence of 0.154 M NaCl, was an ellipsoidal core–shell form factor in combination with Hayter-Penfold structure factor to account for the interaction between charged aggregates of **1**.

The chemical structures of propranolol hydrochloride and its apolar and polar moieties are shown in Fig. 1, and the volumes, atomic scattering lengths, and SLDs of these species are given in Table 1.

2.2.7. Quantum mechanics

As a means to explore the intrinsic geometric preferences for self-interactions of naphthalene rings – as would be expected in the hydrophobic core of any aggregates of the drug formed in solution – gas phase density functional theory calculations were performed using Gaussian16 and employing the M06-2X/6–31 + G* level of theory [50–53]. The molar free energies of the investigated systems (sampled at 298 K) were calculated using GoodVibes [54].

2.2.8. Molecular dynamics

Full atom MD simulations were conducted using Gromacs 2018.4 [55–65] and were performed at a range of concentrations of **1** from 10 mM to 200 mM, employing a simulation box of 15 nm x 15 nm x 15 nm. The simulations were initiated with a random distribution of racemic pairs of drug molecules created using the GMX insert-molecules protocol. Solvent was added using GMX Solvate, and GMX insert-molecules then used to replace randomly selected waters by chloride ions, to balance the number of added drug molecules. The GROMOS 53A6 force field was used, and the parameters for propranolol hydrochloride were obtained *via* PRODRG version AA180301.0717 [66]. The numbers of drug and water molecules included in the simulation box varied with concentration, ranging from 20 and ~108,000 for the 10 mM system, through to 406 and ~103,000 for the 200 mM system. (Full details of the methodology are given in Supplementary Information, Section SI 8).

3. Results and Discussion

3.1. Solubility

In order to establish the concentrations of **1** that might best be investigated in the H/D contrast variation small angle neutron scattering experiments, it was first necessary to measure the drug's solubility in H_2O and D_2O. These measurements were made in quadruplicate at room temperature [67], and the solubilities determined to be 252 ± 7 mM in H_2O, and 133 ± 4 mM in D_2O. The same measurements performed at a

Table 1
Scattering lengths, molecular volumes and scattering length densities of the molecular constituents of the aqueous solvent and drug studied.

Molecule/Fragment	Neutron scattering length, b (10^{-5}Å)	Molecular volume M_v (Å^3)	Scattering length density, ρ (10^{-6}Å^{-2})
Naphthalene ring (protiated) −$C_{10}H_7$	40.28	183[†]	2.20
Naphthalene ring, −$C_{10}D_7$ (d_7, 87 % D)	113.16	183[†]	6.18
Propranolol HCl aliphatic side chain, −$C_6H_{15}ClNO_2$	9.32	264	0.35
Propranolol HCl (protiated) $C_{16}H_{22}ClNO_2$	54.63	447[†]	1.22
Propranolol HCl $C_{16}H_{15}D_7ClNO_2$ (d_7, 88 %D)	127.50	447[†]	2.65
Sodium chloride (NaCl)	13.21	45	2.93
H_2O		30	−0.56
D_2O		30	6.38
0.154 M sodium chloride in D_2O			6.21

[†] volumes calculated from density and molecular weight data. Neutron scattering length density of a molecule/fragment can be calculated by dividing the sum of the scattering length of all atoms in the molecule/fragment by the molecular volume of the molecule/fragment, $\rho = \sum bi/M\nu$

physiological temperature of 310 K, gave the solubilities as 474 ± 14 mM in H_2O, and 375 ± 7 mM in D_2O).

3.2. Surface tension

Measurements of the surface tension were performed for a range of concentrations of **1** in water at room temperature, and parallel experiments were performed with purified **1** dissolved in 0.154 M NaCl.

The slight minimum in the surface tension recorded for purified **1** was found to be smaller than that obtained with the material as purchased (see Supplementary Information), and this is ascribed to the removal of surface active impurities, likely including 1-naphthol, a known contaminant of propranolol [68,69]. Extrapolation of the fits through the experimental data for the low and high concentration regimes gives a point of intersection for the two regression lines that yields an apparent critical micelle concentration (cmc) of 92.4 ± 1.2 mM. This value is of the same order, albeit somewhat lower, than the values (of 100–130 mM) that have been determined using techniques that monitor behaviour in the bulk rather than at the air–water interface [30,39,70].

One would naïvely assume here that the measured apparent cmc of ~ 92 mM marks the start of the formation of aggregates of **1**, while the aqueous solubility of 252 mM marks the upper limit of this regime. As we show below, however, our NMR, small angle scattering, and molecular dynamics studies all show that aggregates (of different sizes and aggregation numbers) are formed even at concentrations well below 92 mM.

3.3. UV spectroscopy

Dilution of **1** with UV spectroscopy monitoring was used to study the very low concentration regime at room temperature, from 0.15 mM down to 0.011 mM (see Supplementary Information, Figure SI 5.1), well below the apparent cmc determined through the surface tension measurements. There are no significant band shifts observable, a finding that might be interpreted as being due to no more than a minor proportion, if any, of **1** self-assembling at concentrations up to 0.15 mM.

3.4. NMR spectroscopy

To probe the solution aggregation of **1**, we collected ^{1}H NMR spectra at room temperature as a function of concentration over the range 2.5 – 180 mM (see Figure SI 6.1). For aggregators, the proton signals of the compound are likely to have concentration-dependent chemical shifts, while for non-aggregators, the peak positions will be independent of concentration [31]. All observed peaks are seen to shift downfield upon dilution due to changes in the magnetic environment of the protons, consistent with the presence of aggregates in solution. In addition, the protons' peak positions shift continuously but variably over the range of the whole titration, indicating a continuous (open) aggregation process occurring at concentrations below the apparent cmc and continuing above it.

All protons on the naphthalene ring experience large shifts during dilution, suggesting their involvement in intermolecular interactions that facilitate the drug's aggregation. Protons 9 and 10 (see Fig. 1) exhibit larger changes in chemical shift than any other aromatic proton, indicating that these protons are intimately involved in these interactions. Since protons 9 and 10 are on the unsubstituted long edge of the naphthyl ring, it is likely that self-aggregation involves significant amounts of edge-to-face CH-π-stacking (T-π geometry) through these two protons. The aliphatic protons also show large concentration-dependent changes in their chemical shifts, possibly indicating intermolecular contacts through electrostatic interactions, hydrogen bonds, or changes in the hydration of the charged group. The splitting pattern of the aliphatic chain is strongly influenced by the stereo-centre on carbon 2 [71] generating an ABMXY spin system [72]. The two diastereotopic protons in positions 1 and 3 show different chemical shifts, which overlap to varying degrees during dilution. Simulated spectra for these five protons (see Figure SI 6.2 and Table SI 6.1) are similar to those observed experimentally. The coupling constants for these protons change monotonically with concentration, though to slightly different extents.

The signals of the diastereotopic methyl protons in the isopropyl group are two doublets at high concentration moving towards overlapping with decreasing concentration (as reported for **1** and other beta-blockers) [73]. The distance of these protons from the stereogenic centre is a cause for the low concentration near-equivalence but formation of aggregates that prevent rotation of the sidechain could enhance differentiation at higher concentration [73]. However, it is also known that in the solid state ^{13}C NMR spectrum, these two methyl carbons give a single broad peak, supporting weak differentiation even when dynamics are restricted [74].

Interpretations in previous NMR studies have assumed a single aggregate size that forms at high concentrations [29,30]. We favour an alternative interpretation in which aggregates of varying sizes are in dynamic equilibrium and, on this assumption, have attempted to fit the data using two models in Bindfit. [75]. The equal *K* (EK) model assumes that additional aggregation proceeds with the same aggregation constant as the initial dimerization whereas for the cooperative equal K (CoEK) model further aggregation is cooperative, in either a positive or negative way, to the initial dimerization with different association constants [76].

The CoEK model was found to give the better fit resulting in a positive binding constant and smaller error and suggests that formation of a **1**-dimer will promote further aggregation. Both of these models are applied because they are tractable but are consistent with a system dominated by either small (dimers) or very large aggregates. The small angle neutron scattering (SANS) data and molecular dynamics (MD) simulations reported below support an alternative interpretation in which the association constant for each increase in aggregate size is different, leading to a distribution of intermediate-sized aggregates. The MD ensembles are consistent with the changes in chemical shift observed indicating the need for a more complex mathematical form than either EK or CoEK to describe this system.

To further explore the aggregation of **1**, 2D ^{1}H NOESY NMR experiments were performed at 180 mM and 50 mM, which are above and below the experimentally determined cmc, respectively. NOESY NMR spectra show inter- and intramolecular interactions of up to 5 Å distance as cross-peaks off the diagonal [77]. The spectrum of the 180 mM solution (Figure SI 6.3a) shows several significant cross peaks, of which intramolecular distances below 5 Å as measured in the single crystal X-ray structure are labelled in black [78]. For the cross peaks labelled in red (for the proton pairs 6 and 9/11, and 8/12), the intramolecular distance is larger than 5 Å such that the appearance of these cross peaks supports the close intermolecular approaches of naphthalene rings. The result coincides with the large shift of protons on the naphthalene ring during dilution. At 50 mM concentration (Figure SI 6.3b), and thus below the cmc measured by any method, the cross peaks labelled in red still exist, suggesting that the interactions *via* the naphthyl ring persist to lower concentration.

3.5. Contrast variation small angle neutron scattering

The SANS profiles of **1** in combination with contrast variation were determined over the concentration range 70 – 200 mM at 298 K. The data were collected on two separate occasions, and on each occasion using freshly prepared samples, in order to check the reproducibility of the profiles. A comparison of the overlaid replicate profiles (presented in Figure SI 7.1) shows that they are gratifyingly consistent, exhibiting no statistically significant differences in their overall topography and levels of absolute scattering.

One set of measured profiles together with the corresponding constrained simultaneous best fits to the data are shown in Fig. 2. Here,

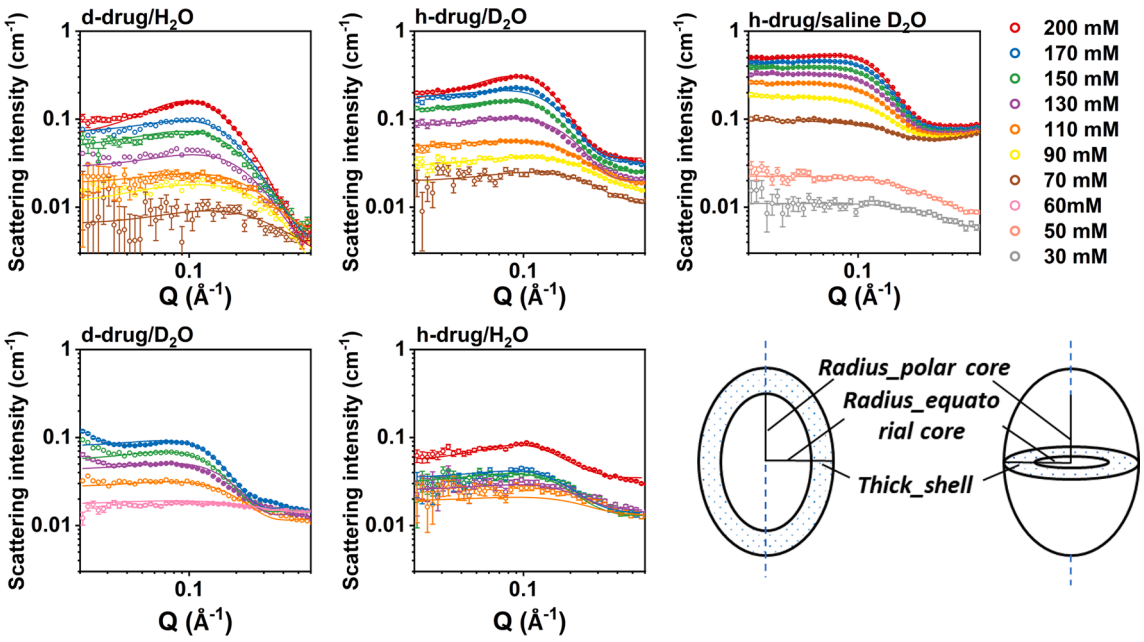

Fig. 2. Upper and Lower Left Panels: SANS data (points) and best constrained simultaneous model fits (solid line) for various contrasts obtained assuming the presence of a core–shell prolate ellipsoid for concentrations of **1** in the range 30 mM – 200 mM. Top Left) d_7 -**1** in H_2O; Top Middle) *h*-**1** in D_2O; Bottom Left) d_7-**1** in D_2O; Bottom Middle) *h*-**1** in H_2O. Top Right) *h*-**1** in D_2O containing 0.154 M NaCl at 298 ± 0.1 K. Lower Right Panel: schematic illustrating the structure of the core–shell prolate ellipsoid used in model-fitting.

contrast variation employed the isotopic composition of water (H_2O vs. D_2O) and of **1** (d_7-**1** involves replacement of each hydrogen on the naphthalene ring with deuterium and *h*-**1** is the protiated equivalent). At the lowest measured concentrations of 70 and 90 mM, two contrasts were used whereas for all higher concentrations, at least three but generally four contrasts were used (see Figure SI 7.2). Additionally, the SANS profile of purified **1** was compared with that obtained for **1**, as purchased, to confirm no significant changes in the SANS profile (Figure SI 7.3) before and after purification.

The parameters used to obtain the best fit to the SANS data for **1** when simultaneously modelled over the measured Q range of 0.02 $Å^{-1}$ to 0.6 $Å^{-1}$ are summarized in Table 2. These parameters are obtained using a core–shell, prolate ellipsoid form factor and a Hayter-Penfold structure factor to account for the repulsive interactions between the charged particles. The modelling assumes a hydrophobic core consisting only of naphthalene rings with no water and therefore permits the aggregation number to be computed assuming a naphthalene volume of 183 $Å^3$.

A low but not irrelevant degree of aggregation is detected at 70 mM, a concentration that is lower than the apparent cmc as measured by any method (*vide supra*). Further, the average aggregation number increases with concentration of **1**, with a larger increase in average aggregation number being seen at higher drug concentrations. This type of behaviour is indicative of a continuous association rather than the classical micelle formation (closed association) that is seen with typical surfactants, such as sodium dodecyl sulfate (SDS), which possess a larger hydrophobic region [79]. The aggregation seen here for **1** is more comparable to that seen with shorter alkyl chain sodium sulfate surfactants [79]. As a consequence of this behaviour, the SANS data in the present study have been corrected for the cmc which means that the average aggregation numbers will include some contribution of molecules in the form of monomers.

Table 2
Structural parameters obtained from the simultaneous best fits to the multiple sets of SANS data using a core–shell prolate ellipsoid model for dispersions of **1** in water at 298 ± 0.1 K.

Solution concentration (mM)	Core equatorial radius (Å)	Core polar radius (Å)	Shell thickness (Å)	Charge (e)	Core volume ($Å^3$)	Shell volume ($Å^3$)	Volume fraction of solvent in shell	Aggregation number in core	Aggregation number in shell
200	6.35 ± 0.02	17.09 ± 0.03	6.13 ± 0.09	5.31 ± 0.03	2883 ± 25	12263 ± 141	0.7	15.8 ± 0.1	15.4 ± 0.1
170	5.99 ± 0.01	16.06 ± 0.05	5.83 ± 0.14	4.74 ± 0.06	2411 ± 17	10396 ± 386	0.7	13.2 ± 0.1	12.7 ± 0.4
150	5.48 ± 0.04	15.76 ± 0.07	5.87 ± 0.16	5.24 ± 0.06	1985 ± 114	9689 ± 412	0.7	10.8 ± 0.6	10.7 ± 1.6
130	5.03 ± 0.05	12.30 ± 0.08	5.36 ± 0.22	1.56 ± 0.08	1303 ± 34	6671 ± 452	0.7	7.1 ± 0.2	6.8 ± 1.8
110	3.89 ± 0.05	11.37 ± 0.14	4.14 ± 0.31	1.26 ± 0.07	720 ± 28	3460 ± 426	0.7	3.9 ± 0.2	3.5 ± 1.2
90	3.68 ± 0.03	8.31 ± 0.06	3.90 ± 0.13	1.77 ± 0.10	472 ± 10	2463 ± 136	0.7	2.6 ± 0.1	2.4 ± 0.6
70	3.51 ± 0.13	7.13 ± 0.18	3.23 ± 0.16	1.79 ± 0.21	369 ± 36	1601 ± 127	0.7	2.0 ± 0.2	1.8 ± 0.3
60	2.96 ± 0.18	6.81 ± 0.32	3.37 ± 0.27	0.85 ± 0.24	249 ± 45	1457 ± 200	0.8	1.4 ± 0.2	1.1 ± 0.2

In parallel with the change in particle size, the average overall charge on the aggregates also increases with concentration of **1**, although the average charge per drug monomer decreases from ~ 0.8 to ~ 0.3 over the same concentration range. This result reflects an increasing degree to which more highly charged, larger aggregates attract more chloride counterions.

The SANS modelling indicates that the side chain of **1** likely resides in the hydrated polar shell region of the aggregates. The value for the scattering length density (SLD) for the shell obtained by modelling (Table 2) allows the solvent content of this region of the aggregate to be estimated. Only the SLDs obtained from the *h*-**1**/D_2O and d_7-**1**/H_2O contrasts were used for these calculations because of their greater difference in contrast between the side chain and solvent. In this way, the volume fractions of solvent in the shell were determined to be in the range 0.7 – 0.8, with the higher concentrations of **1** tending to have slightly lower levels of hydration.

For the low concentration systems, the model-fitted SANS data reveal primarily small aggregates (of ~0.5 nm^3) involving 2 – 7 molecules, but beyond the apparent cmc, the particles increase in size (to ~2.9 nm^3), with aggregation numbers of ~17.

Modelling of the SANS data recorded for the aqueous drug solutions at or above the cmc (*i.e.*, those with concentrations ≥ 90 mM), indicates that the drug associates to form prolate ellipsoidal aggregates with dimensions of around 5 Å x 5 Å x 15 Å. These aggregates carry a small positive charge (of around 5*e*), and they have a 2 – 2.5 nm^3 solvent inaccessible hydrophobic core surrounded by a 5 – 6 Å thick hydrated polar shell. The hydrophobic core comprises the drugs' naphthyl moieties, and the polar shell contains their protonated alkylamine side chains together with ca. 0.7 % v/v bound solvent.

Our SANS studies of the propranolol hydrochloride solutions are the first ever reported on *any* self-associating drug system. There are two previous works in which small X-ray scattering (SAXS) studies have been reported for antidepressant drugs – but neither of these studies (because of the high polydispersity of the drug aggregates and the equivocal fitting of a single contrast of scattering data) proved adequate to furnish any level of detail on the structures of the drug micelles [80,81]. Efthymiou *et al.* showed, by means of SAXS, that the tricyclic antidepressants, amitriptyline, pavatrine, and adiphenine aggregate in aqueous solution to form prolate or oblate ellipsoidal micelles [80], but they were unable to distinguish unambiguously between these two forms on the basis of their quality of fits, and they necessarily neglected to account for solvent associated with the drug aggregates. Similar SAXS studies, with similar limitations, were reported by Perez-Villar for the anti-depressant drug, chlorpromazine [81].

Subsequent analyses focussing on the atomistic detail of the propranolol HCl aggregates was achieved *via* quantum mechanical and molecular dynamics simulations (*vide infra*).

3.6. Quantum mechanical calculations

Given that the aggregates of **1** are shown to have an anhydrous hydrophobic core involving the drug's naphthyl rings, we elected to probe the intrinsic geometric preferences for self-interactions of the naphthalene rings using gas phase density functional theory calculations.

A range of geometries for dimers and trimers were explored (Fig. 3). The lowest energy structure for the dimers was found to be a stacked but offset/twisted arrangement while two other arrangements were found to have free energies within 1 kcal/mol. The calculations support the formation of dimers featuring π-stacked geometries that can differ in the orientation of the rings relative to one another. A study of 1-naphthol dimers using microwave spectroscopy in the gas phase found that the preferred geometry includes π-π stacking but not the alternative hydrogen bonding interaction that could form; in propranolol, therefore, π-π stacking might reasonably be expected to be an important feature [82], although, in solution, solvation effects would undoubtedly perturb the geometric preferences observed in gas phase structures.

The preferred geometry of trimers was probed by taking a π-stacked dimer and adding a third molecule either to continue the stacking or by

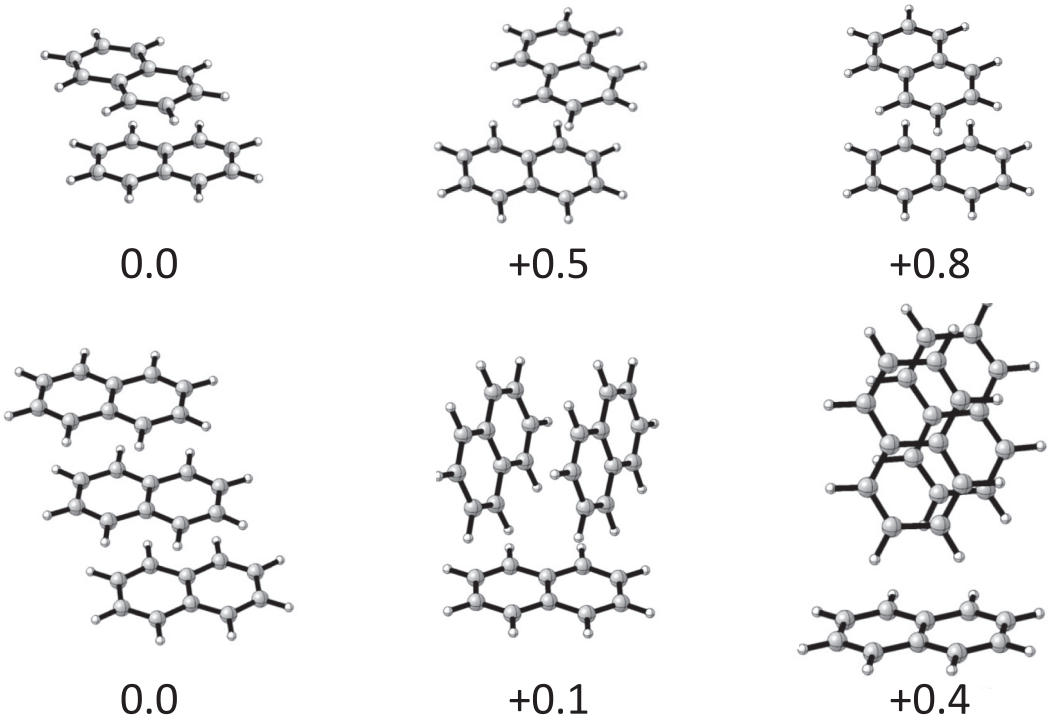

Fig. 3. Top Row (from left to right) shows the three lowest energy geometries for the naphthalene dimer obtained via gas phase density functional theory calculations, as described in the text. All have free energies within 1 kcal/mol of one another. Second Row (from left to right) shows the three lowest energy geometries for the naphthalene trimer obtained by adding a third molecule to a π-π-stacked dimer. Free energies in kcal/mol, expressed relative to the lowest energy arrangement, are given below each structure.

placing its plane such that the ring normal was orthogonal to the ring normal of the two π-stacked rings. The lowest energy structure has a triple stack but is equi-energetic with an arrangement with two CH-π interactions with the stacked rings with the third ring adjacent to the long side of the ring (corresponding to protons 9 and 10 in 1). The alternative with the third molecules adjacent to positions 7 and 8 (or 11 and 12) is 0.3 kcal/mol higher in free energy. The likely lowest energy structure of the naphthalene trimer has no stacking but a threefold symmetry and the tetramer no symmetry [83,84]. This reveals that whereas there is a distinct preference for face-to-face stacking in the naphthalene dimer, this feature is not dominant for larger aggregates. It would be expected, therefore, that aggregates of two molecules would predominantly involve π-π interactions whereas larger aggregates would feature a mixture of π-π and CH-π interactions.

3.7. Molecular dynamics simulations

The MD simulations performed for the various aqueous solutions of **1** were carried out with an initial 200ps run conducted under NVT conditions, with a further 200ps run conducted under NPT conditions, and this was then followed by a further two 20 ns NPT simulations. The equilibration of the system was assessed by monitoring the number of intermolecular interactions between molecules of **1** present during the simulation; equilibration was taken to correspond to this number remaining stable over 20 ns. In most cases, one further 20 ns simulation was required before this equilibration criterion was achieved. An equilibrated 20 ns simulation was treated as the production run for analysis. In all cases, equilibrium was achieved in less than 40 ns and even quite large aggregates were formed before the production run.

The average and mean aggregation numbers obtained at each concentration of **1** from the final production runs are shown in Fig. 4. Graphs of the frequency of aggregates of a particular size over all time points in this run and of the percentage frequency of each aggregate are shown in Figure SI 8.2. Significantly, the molecular dynamics simulations showed that small aggregates (involving up to 5 molecules) appeared even at concentrations of 10 mM, well below the 'apparent' cmc measured by surface tension. These aggregates grow in size as the concentration of **1** increases. The results from the MD simulations correspond well with the SANS and NMR studies in that aggregation was also seen at experimental concentrations below the 'apparent' cmc as determined by surface tension.

When final geometry snapshots of each concentration are classified (*via* the angle formed between ring normals), dimers predominantly feature π-π stacked interactions (88 %), and trimers are also dominated

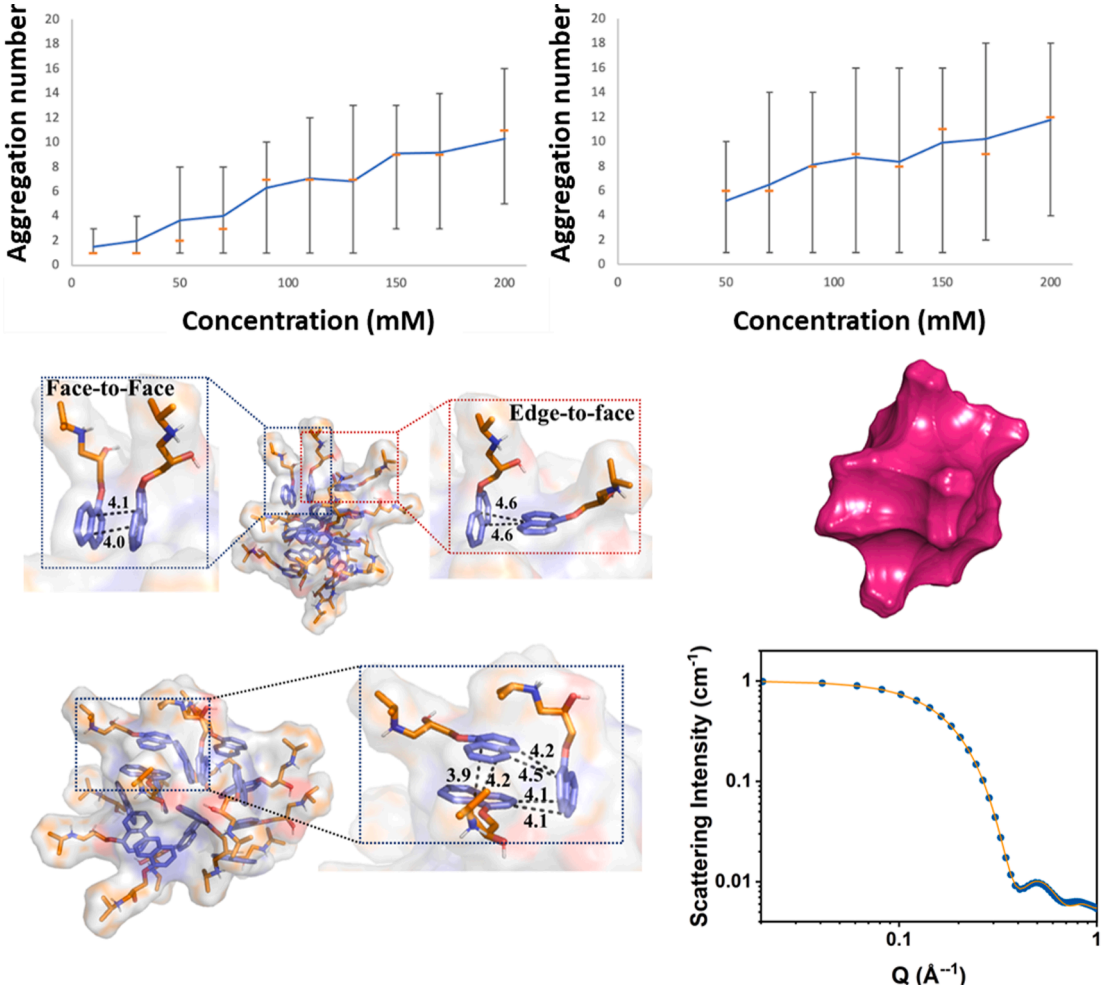

Fig. 4. Top Left) the aggregation number (N_a) measured at each concentration in the molecular dynamics simulations in the absence of NaCl. The solid blue line shows mean values of N_a with orange markers and error bars representing medians and the 10th to 90th percentile range, respectively; Top Right) the same, following addition of 0.154 M NaCl. Bottom left) two representative aggregates with key distances for interactions present in those aggregates in Å. Middle Right) An aggregate enclosed within its solvent-accessible surface, visualized using Accelrys Discovery Studio Visualizer 4.0. Bottom Right) SasCalc computed form factor and SasView model fitted curve for one of the propranolol aggregates (with $N_a = 14$) seen in the equilibrated MD snapshot. The scattering form factor is modelled with the aggregate approximated as a prolate ellipsoid with dimensions, 11.3 Å × 11.3 Å × 16.0 Å. (For interpretation of the references to colour in this figure legend, the reader is referred to the web version of this article.)

by π-π stacking (84 %) but there is a decline in tetramers (70 %) and for larger aggregates approximately equal amounts of both π-π and CH-π interactions prevail. Across all aggregates, there are few extended π-stacking features in which more than three molecules are stacked. Matched and mismatched enantiomers show no difference in propensity for π-π stacking. Fig. 4 shows a typical aggregate composed of 15 drug molecules picked from 200 mM simulations. Consistent with our modelling approach for the SANS data, the aggregate can be regarded as a core–shell structure in which the naphthalene rings constitute the core, with their hydrated chains present in the shell. This core–shell structure can be attributed to the hydrophobic effect and to the specific interactions that the naphthalene moieties make with one another, notably π-π stacking and CH-π interactions. The shortest interatomic distances for π-π and CH-π geometries were measured as ~ 4 Å and 4.6 Å, respectively. In the simulated aggregates, the CH-π geometry was observed only rarely to appear in the absence of a π-π pair, which agrees with the quantum mechanical calculations.

3.8. Linking molecular dynamic simulations to small angle neutron scattering and Nuclear magnetic resonance

The scattering form factors for the individual drug aggregates found in the MD trajectory were calculated using the SasCalc routine as provided in the Sassie program and accessed through the SASSIE-web utility [37,85,86]. The profile of these form factors can then be interpreted as corresponding to regular geometric shapes in the same way as was undertaken for the SANS data via SasView. The aggregation numbers (N_a) of the various aggregates seen in the equilibrated MD snapshot of 200 mM **1** are given in Table SI 9.1, together with their model-fitted ellipsoid semi-axes dimensions (a, b, and c).

Some of the smaller aggregates in the MD ($8 \leq N_a \leq 10$) have SasCalc-computed form factors that are modelled assuming a triaxial ellipsoidal geometry, with dimensions, $a \neq b \neq c$. The larger aggregates, however, that have $N_a \geq 12$, have SasCalc-computed form factors that are modelled assuming a more closely prolate geometry, with $a \approx b \neq c$, $c > a$. Several of the largest aggregates have computed form factors that are fully consistent with a prolate ellipsoidal geometry, having $a = b \neq c$, $c > a$. Given that the measured SANS profiles for the propranolol dispersions will be weighted towards the larger aggregates (that account for a higher volume fraction of the sample), the model-fitted SasCalc predictions of the small angle scattering arising from the aggregates found in the equilibrated MD snapshot are thus found to be gratifyingly consistent with the population ensemble determined by experiment. The MD data provide an atomically detailed representation of the aggregates that is found to be consistent with the SANS data.

The MD simulations reveal that the aggregates are highly dynamic. They form over the course of a few ns; this is also long enough for aggregates to shed molecules (usually but not exclusively, monomers leave). Thus, although NMR spectra could be simulated numerically by assuming a stable equilibrium between monomers and a monodisperse aggregate [30], this is not consistent with our findings or with a system in which collisions between single molecules and aggregates are likely to be diffusion limited. We have therefore processed the MD data in a different way. At each time point, each molecule is classified according to the size of aggregate of which it is a member. A manually determined average chemical shift for molecules in aggregates of that size is assigned. The time-averaged value for each molecule is then computed. The average across all molecules is then obtained. This is performed at each concentration yielding a curve of chemical shift against concentration for each proton type (Section SI 10). The variation of chemical shift with concentration predicted from the MD aggregates overlays reasonably well with the experimentally observed changes. It is reassuring that the MD simulations can realistically represent the experimental observations made by the SANS and NMR measurements.

3.9. Addition of sodium chloride

As a test for this approach, the NMR and SANS experiments as well as the MD simulations were conducted in the presence of 0.154 M NaCl to mimic the ionic strength of physiological fluids. The NMR peak shifts are shown in Figure SI 6.1, the SANS data and the corresponding model fits in Figure SI 7.4 and Table SI 7.3, and the MD aggregate sizes in Figure SI 8.2.

The MD simulations suggest that the aggregates increase in size upon addition of 0.154 M NaCl. Correspondingly the apparent cmc of **1**, determined by surface tension, is reduced from 92.4 mM to 57 ± 1.3 mM in the presence of 0.154 M NaCl (see Figure SI 4.1). In the MD simulations, as the concentration of **1** increases, the effect becomes smaller. At low concentrations the aggregates grow by adding about 2 molecules but at higher concentration, the increase is closer to 1. The mean proportion increase in size is 26 %. A similar but more marked increase is predicted by the Hayter-Penfold interpretation of the SANS data that similarly fits a prolate spheroid (see Table SI 7.3). In this case, these interpretations are generally based on only one contrast although in a limited number of cases, two contrasts were used. As a consequence, the resulting best fits provide a more qualitative guide than for those in the absence of NaCl. The SANS data suggest an increase in aggregate number ranging from 6 to 14, with the biggest increase at intermediate concentrations of **1** (compare Table 2 with Table SI 7.3).

In the NMR spectra, it is clear that the changes in chemical shift as concentration is increased are more pronounced in the presence of NaCl, consistent with formation of larger aggregates. The MD simulations in the presence of NaCl were analysed to arrive at modified chemical shift versus concentration curves while retaining the chemical shifts assigned to each aggregate size. The resulting patterns are consistent with experiment. The change in aggregate composition likely arises because the increased concentration of Na cations in the inter-aggregate space reduces the rate of detachment of monomers from the aggregates.

It is particularly noticeable that in the SANS profiles recorded for 150 – 200 mM of **1** dispersed in 0.154 M NaCl in D_2O, there is an up-turn in the scattering at high *Q*, which is a feature that, to our knowledge, has not been reported previously. It would seem likely that this upturn represents the leading edge of a wide-angle peak – centred around 1 – 1.5 $Å^{-1}$ (and thus corresponding to spacings of the order of ~ 6 Å). This might be due to interactions between the aromatic moieties of the aggregated drug molecules, as seen, for example, in the solution scattering profiles recorded for pyridine and naphthalene and surfactant/perfume aggregates [87–90]. Alternatively, the feature might arise because of a change in drug-solvent and/or drug-counterion interactions caused by the presence of the added NaCl. There is no such up-turn seen in the high-*Q* scattering for the SANS profiles recorded for the 30 mM and 50 mM dispersions of **1** in D_2O/saline, which suggests that the naphthyl rings are more randomly arranged in the smaller and/or more short-lived aggregates present in these systems and/or that there is a change in the organization of the solvent or counterions surrounding these aggregates. Whatever the origin(s) of the upturn seen in the scattering profiles of the D_2O/saline drug dispersions, it is interesting to note that its absence in the profiles recorded at low drug concentrations is consistent with the lower cmc observed in the presence of 0.154 M NaCl (*vide supra*). Interestingly, however, due to an absence of the up-turn in the scattering at high *Q*, it only proved possible to fit the SANS data for **1** at 50 and 30 mM using an ellipsoid form factor and associated Hayter-Penfold structure factor model, suggesting that either the naphthalene rings were too far apart for their interaction to be seen and/or there is a change in packing seen at low drug concentrations. The absence of an up-turn at these low concentrations agrees with the low cmc observed in the presence of 0.154 mM NaCl.

3.10. Single enantiomer studies and the solid state

We have also considered the possible connection between these

solution aggregates and the molecular structure of the solid state. Previous studies have established that racemic **1** has at least three crystalline forms [91,92], of which one form has been characterized by single crystal X-ray diffraction. While initially the crystal structure of the racemate was solved in the centrosymmetric space groups $P2_1/c$ or $P2_1/n$ [93,94], this was later revised to the chiral space group $P2_1$ with two symmetry-independent enantiomeric molecules in the asymmetric unit [77]. There are suggestions that racemic **1** can crystallize as a conglomerate as well as in a racemic crystal form [77,95], while the racemate looks to be preferred [77,91,96]. In the most recent studies, the structure is observed to consist of two independent chains, each of which contains only one enantiomer while the interactions between these two chains are hydrophobic. Key organising interactions in all structures are assigned to electrostatic and dipole-charge interactions between the ammonium centre and/or the alcohol in **1** with chloride anions. These two properties are illustrated in Fig. 5 with the two enantiomers colour coded and interactions with chloride highlighted.

It is noticeable that the opposite trends are seen in the solution phase structures from the MD of the racemate, as illustrated by radial distribution functions (RDFs) for chlorides around the amine nitrogen atoms

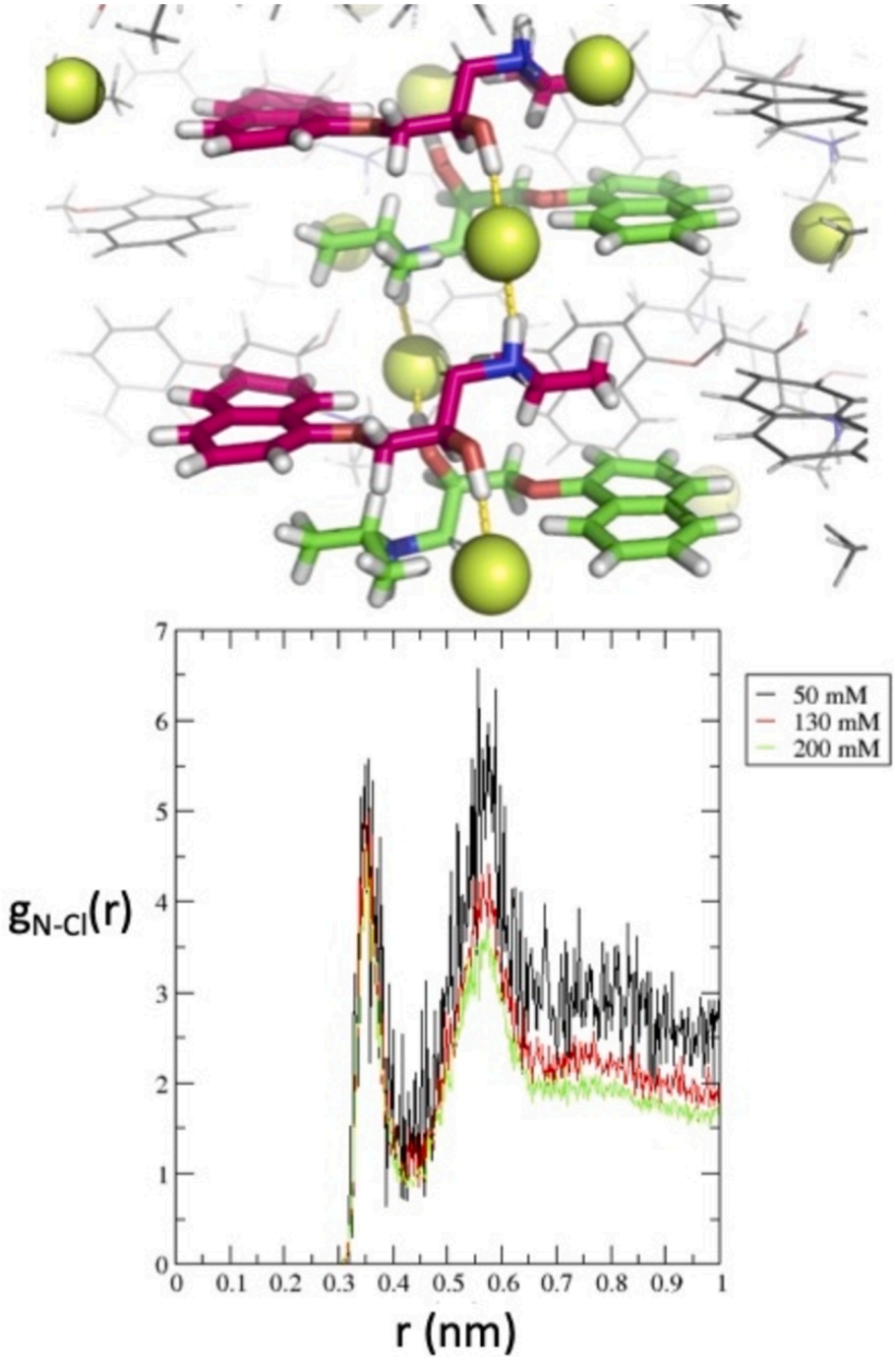

Fig. 5. Top: The crystal structure of **1** (CCDC Refcode, FIDGAB) is shown with carbons colour coded according to enantiomer as capped sticks and chloride ions shown as spheres in yellow [44]. Bottom: The radial distribution function for chloride ions around the protonated amines computed for MD simulations at concentrations of 50 mM (black), 130 mM (red) and 200 mM (green). (For interpretation of the references to colour in this figure legend, the reader is referred to the web version of this article.)

(Fig. 5). The first feature in the RDF is centred around 0.32 nm and represents the hydrogen bond donated from the amino moiety to chloride, like that observed in the solid state. The sharpness and narrow distribution indicates that this strong interaction also persists in solution. The second feature centred around 0.57 nm likely represents the distance between the amino nitrogen atom and the chloride ion hydrogen bonded to the vicinal alcohol and indicates the presence of small chains as can also be seen in the crystal structure (distance of 0.54 nm). Surprisingly, the second feature decreases in intensity with increasing concentration indicating that these small chains are broken, likely due to the curvature of the aggregates present.

Finally, SANS data of both single enantiomers separately were measured for two contrasts at 110, 130 and 150 mM (see Figure SI 7.4 and Table SI 7.2) and MD was performed at 200 mM (Section SI 8). Both studies show that single enantiomers exhibit similar behaviour to that of the racemate.

Although molecular aggregation is evident in solution, the direct comparison between these aggregates and the dominant structures in the solid-state show that significant reorganization has to happen during the nucleation step. While crystallization of both the racemic and the enantiomerically pure propranolol hydrochloride from solution is not hindered, it is likely that nucleation follows a non-classical pathway with the phase separation of a dense liquid (comparable to the clusters observed) already occurring at undersaturated concentrations [44].

4. Conclusions

Through the combined application of multiple experimental and theoretical methodologies, we have herein provided the first fully comprehensive – nanoscale – description of the aqueous solution phase behaviour of the beta-blocker drug, propranolol hydrochloride, exploring solution concentrations ranging from 2.5 mM to 200 mM. Some of the principal features found are summarized in the schematic shown in Fig. 6.

As was demonstrated by earlier authors [30,39,53,97–99], we find that the drug self-associates in solution, exhibiting discontinuities in its surface tension and ^{1}H NMR shift change profiles that are consistent with the formation of micelle-like aggregates above a certain, critical concentration. This apparent critical aggregation/micelle concentration (cmc), as calculated from the surface tension and NMR measurements reported here, is consistent with the corresponding values reported previously by others, and the aggregation numbers we have determined through modelling of our reported SANS data are also consistent (Table 3).

By means of our small angle neutron scattering (SANS) studies (and exploiting the device of H/D contrast variation), however, we have also obtained unequivocal evidence that the drug forms aggregates even at concentrations below the cmc. Moreover, the size, shape, and aggregation numbers of the aggregates are not only found to vary with drug concentration but are also seen to be influenced by the presence of added sodium chloride.

Molecular dynamics (MD) simulations of such systems are rare and are confined – to the best of our knowledge – just to a single report, presented by Kozlowska *et al.* [100], detailing the aggregation behaviour in aqueous solution of just a single concentration of the non-steroidal anti-inflammatory drug, diclofenac.

The MD simulations performed here on the propranolol hydrochloride systems, have been performed for a whole range of drug

Table 3
Comparison of parameters reported here and in the literature for propranolol hydrochloride micelles.

Measurement technique	Reference	Micelle aggregation number		Critical micelle concentration / mmol kg^{-1}	
		Literature	This work*	Literature	This work
Surface tension	[97,98]	–	4 – 16	95–97	92
Light scattering	[30]	10		124	–
Conductivity	[39]	10		128–130	–
Ultrasound velocity	[53,99]	–		131	–
NMR	[30]	15		88 – 108	90 – 95†

† calculated from the minima seen in plots of the second derivative of chemical shift changes *vs.* concentration for protons 4, 6 and 10 (see Fig. 1); data not shown.
* calculated from models fitted to SANS data measured for solutions with concentrations ranging from 90 – 200 mM.

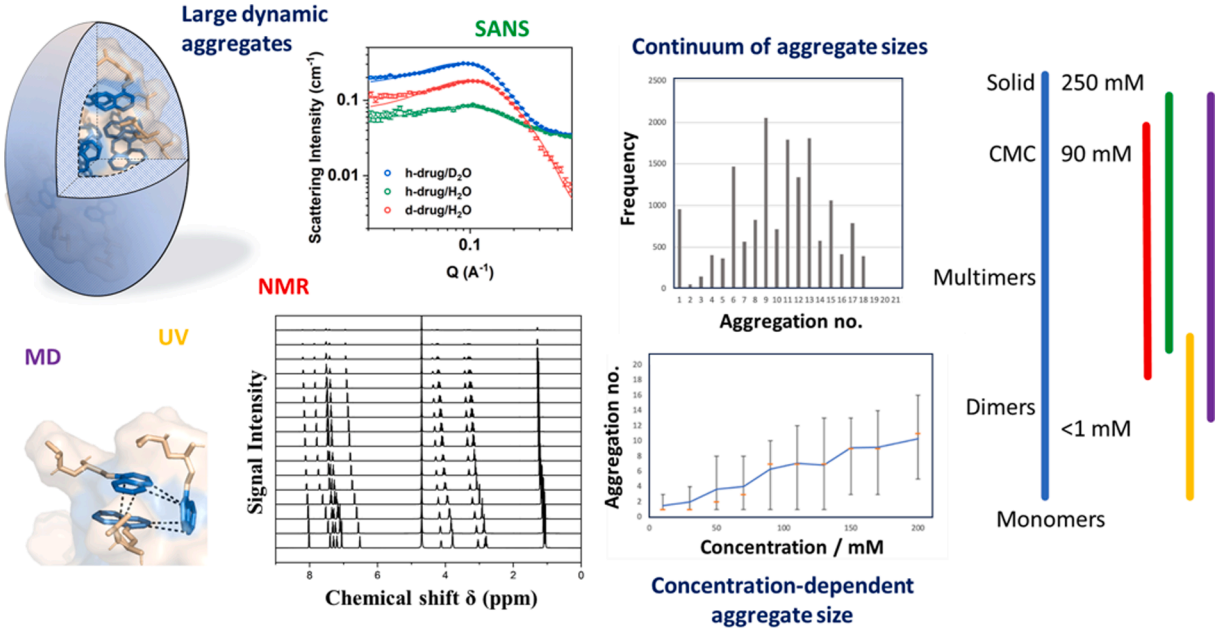

Fig. 6. Schematic illustration summarising the findings from the multiple experimental and theoretical techniques brought to bear in studying the self-association of propranolol hydrochloride in aqueous solution.

concentrations, and are shown to be gratifyingly consistent with our measured SANS data, with the scattering profiles back calculated from the atomic co-ordinates indicating aggregates of broadly similar shape and size.

The MD simulations also show, however, that a *continuum* of particle sizes exists across the *whole* of the concentration range studied beyond 10 mM, and this again is consistent with the findings from our SANS experiments. This continuous self-association behaviour has been demonstrated experimentally for various phenothiazine drugs [101–103], but it has not been reported before for propranolol. That said, we have confidence that the MD simulations realistically model the behaviour of the real-world systems because, over and above the agreement seen between the MD and SANS, we also find agreement between the MD and our NMR data. More specifically, we see that when the aggregates found in the simulations are used in modelling the concentration-dependent patterns of change in the drug's ^{1}H NMR chemical shifts, the predicted and experimentally observed patterns agree closely. In performing these calculations, we took – as observed – that there exists a dynamic equilibrium between aggregates of different sizes within the solutions and, contrary to the assumptions made on the equal K and co-operative equal K formalisms, we assumed that the association constant for each increase in aggregate size is different. Such treatment is consistent with the *N*-dependent increase in association constant (K_N) reported by Attwood *et al* for the self-association of a trimethoxyhexadecyl polyoxyethylene glycol monoether surfactant [103], and also that reported by Attwood & Fletcher [104] for the drug, trimetaphan camphorsulfonate.

Given the level of agreement thus found between the MD modelling of the propranolol systems and the corresponding SANS and NMR measurements, we moved to interrogate the former to provide a more detailed (atomistic) description of the systems' behaviour, and thence to relate the intermolecular arrangements found within the aggregates to the packing of propranolol molecules observed in the solid state.

In the smaller aggregates seen in the MD trajectories (involving 2 – 4 drug molecules), the naphthyl rings are found to interact predominantly via π-π stacking, whereas the larger ones (involving six or more molecules) feature approximately equal proportions of π-π and CH-π interactions. Such differences in the self-interacting naphthalene ring geometries are supported by the results obtained in our DFT quantum mechanical calculations.

As the concentration of drug is raised above that corresponding to the apparent cmc determined though surface tension measurements, more complex, dynamic aggregates are seen to form that involve rapid addition and loss of matter, mostly in the form of monomers colliding or detaching, both processes occurring on a nanosecond timescale. These mesoscale aggregates can be viewed as large molecular clusters or as very small droplets of liquid surrounded by a distinct liquid phase; they bridge these two domains. The large aggregates notably lack key features present in the solid state drug and this would suggest that there is a restructuring of these species required before any nucleation of solid.

In consequence of these findings and given the numerous ways in which the aggregation of small molecule pharmaceuticals like propranolol can impact their development, their formulation, and their utility as medicines (*vide supra*), we conclude with a note of caution. Over the last two decades there have been numerous authors advocating that aggregators should be disfavoured from consideration in high-throughput screening for potential new drug candidates [105–108]. We would urge caution: there remains much that is yet to be determined about the nature of aggregation and of the transition from solution to solid phase. As we have shown here, a more complete understanding of these processes can be gained by applying multiple methods for characterisation, and by combining experiment with computer modelling. It is by these means that we gain a complete picture of solution phase behaviours and, in respect of pharmaceuticals specifically, can formulate evidence-based decisions regarding the suitability of screened compounds to be progressed for development.

CRediT authorship contribution statement

Yixuan Yan: Writing – review & editing, Writing – original draft, Visualization, Investigation, Data curation. **Yichun Shen:** Writing – review & editing, Visualization, Investigation, Data curation. **Najet Mahmoudi:** Writing – review & editing, Investigation. **Peixun Li:** Writing – review & editing, Investigation. **James Tellam:** Writing – review & editing, Investigation. **Richard A. Campbell:** Writing – review & editing. **David J. Barlow:** Writing – review & editing, Writing – original draft, Visualization, Methodology, Investigation, Formal analysis, Data curation, Conceptualization. **Katharina Edkins:** Writing – review & editing, Writing – original draft, Visualization, Supervision, Methodology, Investigation, Funding acquisition, Data curation, Conceptualization. **Andrew G. Leach:** Writing – review & editing, Writing – original draft, Visualization, Supervision, Methodology, Investigation, Funding acquisition, Formal analysis, Data curation, Conceptualization. **M.Jayne Lawrence:** Writing – review & editing, Writing – original draft, Visualization, Supervision, Project administration, Methodology, Investigation, Funding acquisition, Data curation, Conceptualization.

Declaration of competing interest

The authors declare that they have no known competing financial interests or personal relationships that could have appeared to influence the work reported in this paper.

Acknowledgements

The authors would like to acknowledge the assistance given by Research IT and the use of the Computational Shared Facility at The University of Manchester. YS thanks the China Scholarship Council (CSC) (202006250018) for funding. YY thanks the China Scholarship Council (CSC) (201806180016). Experiments at the ISIS Neutron and Muon Source were supported by beamtime allocation from STFC, and the SANS data are available at DOIs: 10.5286/ISIS.E.RB2010651-2. This work benefited from the use of the SasView application, originally developed under National Science Foundation Award DMR-0520547. SasView also contains a code developed with funding from the European Union's Horizon 2020 research and innovation program under the SINE2020 project, Grant No. 654000. MJL thanks Professor David Attwood for all the help and encouragement he gave to her as an early career researcher and for opening her eyes to how many drugs self-assemble.

Appendix A. Supplementary data

Supplementary data to this article can be found online at https://doi.org/10.1016/j.jcis.2024.12.131.

Data availability

Data will be made available on request.

References

[1] R.R.E. Steendam, U.B.R. Khandavilli, L. Keshavarz, P.J. Frwley, *Solution versus crystal hydration: the case of gamma-amino acid pregabalin*, Cryst. Growth Des. 19 (2019) 4483–4488, https://doi.org/10.1021/acs.cgd.9b00253.

[2] A.T. Florence, R.T. Parfitt, *Nuclear magnetic resonance studies on micelle formation by promethazine hydrochloride*, J. Pharm. Pharmacol. 22 (1970) S121, https://doi.org/10.1111/j.2042-7158.1970.tb08590.x.

[3] A.T. Florence, R.T. Parfitt, *Micelle formation by some phenothiazine derivatives. II. Nuclear magnetic resonance studies in deuterium oxide*, J. Phys. Chem. 75 (1971) 3554–3560, https://doi.org/10.1021/j100692a012.

[4] S. Schreier, S.V.P. Malheiros, E. de Paula, *Surface active drugs: self-association and interaction with membranes and surfactants. Physicochemical and biological aspects*, Biochim. Biophys. Acta 1508 (2000) 210–234, https://doi.org/10.1016/S0304-4157(00)00012-5.

[5] A.T.M. Serajuddin, *Salt formation to improve drug solubility*, Adv. Drug Del. Rev. 59 (2007) 603–616, https://doi.org/10.1016/j.addr.2007.05.010.

[6] Y.A. Abramov, P.Y. Zhang, Q. Zeng, M.J. Yang, Y. Liu, S. Sekharan, *Computational insights into kinetic hindrance affecting crystallization of stable forms of active pharmaceutical ingredients*, Crystal Growth Design 20 (2020) 1512–1525, https://doi.org/10.1021/acs.cgd.9b01153.

[7] D.K. Bucar, R.W. Lancaster, J. Bernstein, *Disappearing polymorphs revisited*, Ang. Chemie Intl. Ed. 54 (2015) 6972–6993, https://doi.org/10.1002/anie.201410356.

[8] T. Kikuchi, N. Ito, H. Sasaki, *Self-association properties of 4-[1-hydroxy-1-methyl-ethyl]-2-propyl-1-[4-[2-[tetrazole-5-yl]phenyl]phenyl] methylimidazole-5-carboxylic acid monohydrate (CS-088), an antiglaucoma ophthalmic agent*, Int. J. Pharm. 299 (2005) 100–106, https://doi.org/10.1016/j.ijpharm.2005.04.035.

[9] Q.A. Khan, C.M. Barbieri, A.R. Srinivasan, Y.H. Wang, E.J. LaVoie, D.S. Pilch, *Drug self-association modulates the cellular bioavailability of DNA minor groove-directed terbenzimidazoles*, J. Med. Chem. 49 (2006) 5245–5251, https://doi.org/10.1021/jm060520q.

[10] A. Seelig, R. Gottschlich, R.M. Devant, *A method to determine the ability of drugs to diffuse through the blood-brain barrier*, Proc. Natl. Acad. Sci. (USA) 91 (1994) 68–72, https://doi.org/10.1073/pnas.91.1.68.

[11] R. Inacio, D. Barlow, X. Kong, J. Keeble, S.A. Jones, *Investigating how the attributes of self-associated drug complexes influence the passive transport of molecules through biological membranes*, E. J. Pharm. Biopharm. 102 (2016) 214–222, https://doi.org/10.1016/j.ejpb.2016.03.002.

[12] D.B. Goldstein, *The effects of drugs on membrane fluidity*, Ann. Rev. Pharmacol. Toxicol. 24 (1984) 43–64, https://doi.org/10.1146/annurev.pa.24.040184.000355.

[13] A.M. Davis, S.A. St-Gallay, G.J. Kleywegt, *Limitations and lessons in the use of X-ray structural information in drug design*, Drug Discov. Today. 13 (19–20) (2008) 831–841, https://doi.org/10.1016/j.drudis.2008.06.006.

[14] S.R. LaPlante, V. Roux, F. Shahout, G. LaPlante, S. Woo, M.M. Denk, S.T. Larda, Y. Ayotte, *Probing the free-state solution behavior of drugs and their tendencies to self-aggregate into nano-entities*, Nat. Protoc. 16 (11) (2021) 5250–5273, https://doi.org/10.1038/s41596-021-00612-3.

[15] Kumar, A.; Krishna; Sharma, A.; Dhankhar, J.; Syeda, S.; Shrivastava, A.; Sharma, S. K. (2022) *Self-Assembly and Transport Behaviour of Non-ionic Fluorinated and Alkylated Amphiphiles for Drug Delivery*. ChemistrySelect, **7** (35), e202203274. doi: 10.1002/slct.202203274.

[16] L. Zhang, L. Gao, Q. Liu, F. Yang, Y. Fang, *A novel surfactant-like fluorophore and its probing ability to the aggregation of amphiphilic compounds*, J. Photochem. Photobiol. A 245 (2012) 58–65, https://doi.org/10.1016/j.jphotochem.2012.07.001.

[17] A. Yousefi, S.A. Aslanzadeh, J. Akbari, *Effect of 1-ethyl-3-methylimidazolium bromide on interfacial and aggregation behavior of mixed cationic and anionic surfactants*, J. Mol. Liq. 219 (2016) 637–642, https://doi.org/10.1016/j.molliq.2016.03.076.

[18] Y. Wei, F. Cheng, G. Hou, S. Sun, *Amphiphilic cellulose: Surface activity and aqueous self-assembly into nano-sized polymeric micelles*, React. Polym. 68 (5) (2008) 981–989, https://doi.org/10.1016/j.reactfunctpolym.2008.02.004.

[19] Z.S. Vaid, S.M. Rajput, A. Shah, Y. Kadam, A. Kumar, O.A. El Seoud, J.P. Mata, N. I. Malek, *Salt-Induced Microstructural Transitions in Aqueous Dispersions of Ionic-Liquids-Based Surfactants*, ChemistrySelect 3 (17) (2018) 4851–4858, https://doi.org/10.1002/slct.201800041.

[20] B. Sitharaman, S. Asokan, I. Rusakova, M.S. Wong, L.J. Wilson, *Nanoscale Aggregation Properties of Neuroprotective Carboxyfullerene (C3) in Aqueous Solution*, Nano Lett. 4 (9) (2004) 1759–1762, https://doi.org/10.1021/nl049315t.

[21] G. Pinedo-Martín, M. Santos, A.M. Testera, M. Alonso, J.C. Rodríguez-Cabello, *The effect of NaCl on the self-assembly of elastin-like block co-recombinamers: Tuning the size of micelles and vesicles*, Polymer 55 (21) (2014) 5314–5321, https://doi.org/10.1016/j.polymer.2014.08.053.

[22] B. Jin, Z. Liu, R. Tang, *Recent experimental explorations of non-classical nucleation*, CrstEngComm 22 (24) (2020) 4057–4073, https://doi.org/10.1039/D0CE00480D.

[23] J. Wang, S. Han, G. Meng, H. Xu, D. Xia, X. Zhao, R. Schweins, J.R. Lu, *Dynamic self-assembly of surfactant-like peptides A6K and A9K*, Soft Matter 5 (20) (2009), https://doi.org/10.1039/b901653h.

[24] A.K. Naik, S.P. Biswal, P. Hota, M. Mithilesh, M. Saxena, P.K. Misra, *Ion-Adduct with Hydrophobic Scaffold: Synthesis, Characterization and Solution Behaviour*, Mater. Today: Proc. 9 (2019) 568–577, https://doi.org/10.1016/j.matpr.2018.10.377.

[25] J. Zhu, L. Li, L. Chen, X. Li, *Nano-structure of octenyl succinic anhydride modified starch micelle*, Food Hydrocoll. 32 (1) (2013) 1–8, https://doi.org/10.1016/j.foodhyd.2012.11.033.

[26] M.A. Lebedeva, E. Palmieri, P. Kukura, S.P. Fletcher, *Emergence and Rearrangement of Dynamic Supramolecular Aggregates Visualized by Interferometric Scattering Microscopy*, ACS Nano 14 (9) (2020) 11160–11168, https://doi.org/10.1021/acsnano.0c02414.

[27] A.V. Orlova, D.A. Ahiadorme, T.V. Laptinskaya, L.O. Kononov, *Supramer analysis of 2,3,5-tri-O-benzoyl-α-d-arabinofuranosyl bromide solutions in different solvents: supramolecular aggregation of solute molecules in 1,2-dichloroethane mediated by halogen bonds*, Russ. Chem. Bull. 70 (11) (2022) 2214–2219, https://doi.org/10.1007/s11172-021-3335-8.

[28] J. Marcus, D. Touraud, S. Prevost, O. Diat, T. Zemb, W. Kunz, *Influence of additives on the structure of surfactant-free microemulsions*, Phys. Chem. Chem. Phys. 17 (48) (2015) 32528–32538, https://doi.org/10.1039/C5CP06364G.

[29] Ruso, J. M.; Taboada, P.; Attwood, D.; Mosquera, V.; Sarmiento, F. l. (2000) Determination of the aggregation properties of weakly self-associating systems by NMR techniques: the self-association of propranolol hydrochloride in aqueous electrolyte solution. Phys. Chem. Chem. Phys., **2** (6), 1261-1265. doi: 10.1039/A909407E.

[30] J.M. Ruso, D. Attwood, C. Rey, P. Taboada, V. Mosquera, F. Sarmiento, *Light Scattering and NMR Studies of the Self-Association of the Amphiphilic Molecule Propranolol Hydrochloride in Aqueous Electrolyte Solutions*, J. Phys. Chem., B 103 (34) (1999) 7092–7096, https://doi.org/10.1021/jp983900z.

[31] S.R. LaPlante, R. Carson, J. Gillard, N. Aubry, R. Coulombe, S. Bordeleau, P. Bonneau, M. Little, J. O'Meara, P.L. Beaulieu, *Compound Aggregation in Drug Discovery: Implementing a Practical NMR Assay for Medicinal Chemists*, J. Med. Chem. 56 (12) (2013) 5142–5150, https://doi.org/10.1021/jm400535b.

[32] Calandra, P.; Turco Liveri, V.; Ruggirello, A. M.; Licciardi, M.; Lombardo, D.; Mandanici, A. (2015) *Anti-Arrhenian behaviour of conductivity in octanoic acid–bis (2-ethylhexyl)amine systems: a physico-chemical study*. J. Mater. Chem., C, **3** (13), 3198-3210. doi: 10.1039/C4TC02500H.

[33] W. Murakami, A. De Nicola, Y. Oya, J.-I. Takimoto, M. Celino, T. Kawakatsu, G. Milano, *Theoretical and Computational Study of the Sphere-to-Rod Transition of Triton X-100 Micellar Nanoscale Aggregates in Aqueous Solution: Implications for Membrane Protein Purification and Membrane Solubilization*, ACS Appl. Nano Mater. 4 (5) (2021) 4552–4561, https://doi.org/10.1021/acsanm.1c00171.

[34] D. Bochicchio, G.M. Pavan, *From Cooperative Self-Assembly to Water-Soluble Supramolecular Polymers Using Coarse-Grained Simulations*, ACS Nano 11 (1) (2017) 1000–1011, https://doi.org/10.1021/acsnano.6b07628.

[35] A. Paquet, O. Diat, L. Berthon, P. Guilbaud, *Aggregation in organic phases after solvent extraction of uranyl nitrate: X-ray scattering and molecular dynamic simulations*, J. Mol. Liq. 277 (2019) 22–35, https://doi.org/10.1016/j.molliq.2018.12.051.

[36] K.A. Rubinson, P. Buhlmann, T.C. Allison, *One-dimensional ionic self-assembly in a fluorous solution: the structure of tetra-n-butylammonium tetrakis[3,5-bis (perfluorohexyl)phenyl]borate in perfluoromethylcyclohexane by small-angle neutron scattering (SANS)*, Phys. Chem. Chem. Phys. 18 (14) (2016) 9470–9475, https://doi.org/10.1039/C6CP00393A.

[37] J.E. Curtis, S. Raghunandan, H. Nanda, S. Krueger, *SASSIE: A program to study intrinsically disordered biological molecules and macromolecular ensembles using experimental scattering restraints*, Comput. Phys. Commun. 183 (2) (2012) 382–389, https://doi.org/10.1016/j.cpc.2011.09.010.

[38] N. Zec, G. Mangiapia, A.C. Hendry, R. Barker, A. Koutsioubas, H. Frielinghaus, M. Campana, J.L. Ortega-Roldan, S. Busch, J.F. Moulin, *Mutually Beneficial Combination of Molecular Dynamics Computer Simulations and Scattering Experiments*, Membranes 11 (7) (2021), https://doi.org/10.3390/membranes11070507.

[39] V.V. Mosquera, J.M. Ruso, D. Attwood, M.N. Jones, G. Prieto, F. Sarmiento, *Thermodynamics of Micellization of Surfactants of Low Aggregation Number: The Aggregation of Propranolol Hydrochloride*, J. Colloid Interface Sci. 210 (1) (1999) 97–102, https://doi.org/10.1006/jcis.1998.5948.

[40] D.G. Shand, *Drug therapy: Propranolol*, N. Engl. J. Med. 293 (6) (1975) 280–285, https://doi.org/10.1056/NEJM197508072930606.

[41] A.A. Al-Majed, A.H.H. Bakheit, H.A. Abdel Aziz, F.M. Alajmi, H. AlRabiah, *Propranolol*, Profiles Drug. Subst. Excip. Relat. Methodol. 42 (2017) 287–338, https://doi.org/10.1016/bs.podrm.2017.02.006.

[42] Jones, C. D.; Walker, M.; Xiao, Y.; Edkins, K. *Pre-nucleation aggregation based on solvent microheterogeneity*. Chem. Commun., **55** (33), 4865-4868. doi: 10.1039/c9cc01455a.

[43] Y. Zhang, I.R. Turkmen, B. Wassermann, A. Erko, E. Ruhl, *Structural motifs of pre-nucleation clusters*, J. Chem. Phys. 139 (13) (2013) 134506, https://doi.org/10.1063/1.4823497.

[44] D. Gebauer, M. Kellermeier, J.D. Gale, L. Bergstrom, H. Colfen, *Pre-nucleation clusters as solute precursors in crystallisation*, Chem. Soc. Rev. 43 (7) (2014) 2348–2371, https://doi.org/10.1039/c3cs60451a.

[45] A.S. Patil, A.A. Shirkhedkar, S.J. Surana, P.S. Nawale, *Q-absorbance and multicomponent UV spectrophotometric methods for simultaneous estimation of propranolol hydrochloride and flunarizine dihydrochloride in capsules*, Der Pharma Chemica 3 (3) (2011) 404–408.

[46] J.B. Hayter, J. Penfold, *Determination of micelle structure and charge by neutron small-angle scattering*, Colloid Polym. Sci. 261 (12) (2006) 1022–1030, https://doi.org/10.1007/bf01421709.

[47] J.B. Hayter, J. Penfold, *An analytic structure factor for macroion solutions*, Mol. Phys. 42 (1) (2006) 109–118, https://doi.org/10.1080/00268978100100091.

[48] J.K. Percus, G.J. Yevick, *Analysis of Classical Statistical Mechanics by Means of Collective Coordinates*, Phys. Rev. 110 (1) (1958) 1–13, https://doi.org/10.1103/PhysRev.110.1.

[49] Doucet, M., Cho, J.H., Alina, G., Bakker, J., Bouwman, W., Butler, P., Campbell, K., Gonzales, M., Heenan, R., Jackson, A., Juhas, P., King, S., Kienzle, P., Krzywon, J., Markvardsen, A., Nielsen, T., O'Driscoll, L., Potrzebowski, W., Ferraz Leal, R., Richter, T., Rozycko, P., Snow, T., Washington, A. *SasView version 4.2*. 2018. doi: 10.5281/zenodo.1412041.

[50] Y. Zhao, D.G. Truhlar, *Density functionals with broad applicability in chemistry*, Acc. Chem. Res. 41 (2) (2008) 157–167, https://doi.org/10.1021/ar700111a.

[51] Y. Zhao, D.G. Truhlar, *The M06 suite of density functionals for main group thermochemistry, thermochemical kinetics, noncovalent interactions, excited states, and transition elements: two new functionals and systematic testing of four M06-class functionals and 12 other functionals*, Theor. Chem. Acc. 120 (1–3) (2007) 215–241, https://doi.org/10.1007/s00214-007-0310-x.

[52] R. Krishnan, J.S. Binkley, R. Seeger, J.A. Pople, *Self-consistent molecular orbital methods. XX. A basis set for correlated wave functions*, J. Chem. Phys. 72 (1) (1980) 650–654, https://doi.org/10.1063/1.438955.

[53] P.C. Hariharan, J.A. Pople, *The influence of polarization functions on molecular orbital hydrogenation energies*, Theor. Chim. Acta 28 (3) (1973) 213–222, https://doi.org/10.1007/bf00533485.

[54] G. Luchini, J.V. Alegre-Requena, I. Funes-Ardoiz, R.S. Paton, *GoodVibes: Automated Thermochemistry for Heterogeneous Computational Chemistry Data*. F1000Research (2020) 9, https://doi.org/10.12688/f1000research.22758.1.

[55] M.J. Abraham, T. Murtola, R. Schulz, S. Páll, J.C. Smith, B. Hess, E. Lindahl, *GROMACS: High performance molecular simulations through multi-level parallelism from laptops to supercomputers*, SoftwareX 1–2 (2015) 19–25, https://doi.org/10.1016/j.softx.2015.06.001.

[56] Bekker, H.; Berendsen, H. J. C.; Dijkstra, E. J.; Achterop, S.; Vondrumen, R.; Vanderspoel, D.; Sijbers, A.; Keegstra, H.; Renardus, M. K. R. (1993) *Gromacs-a parallel computer for molecular-dynamics simulations*.; World Scientific Publishing: pp 252-256. ISBN 981-02-1245-3.

[57] H.J.C. Berendsen, D. van der Spoel, R. van Drunen, *GROMACS: A message-passing parallel molecular dynamics implementation*, Comput. Phys. Commun. 91 (1–3) (1995) 43–56, https://doi.org/10.1016/0010-4655(95)00042-e.

[58] B. Hess, C. Kutzner, D. van der Spoel, E. Lindahl, *GROMACS 4: Algorithms for Highly Efficient, Load-Balanced, and Scalable Molecular Simulation*, J. Chem. Theory Comput. 4 (3) (2008) 435–447, https://doi.org/10.1021/ct700301q.

[59] E. Lindahl, B. Hess, D. van der Spoel, *GROMACS 3.0: a package for molecular simulation and trajectory analysis*, J. Mol. Modeling 7 (8) (2001) 306–317, https://doi.org/10.1007/s008940100045.

[60] Páll, S.; Abraham, M. J.; Kutzner, C.; Hess, B.; Lindahl, E. (2015) *Tackling Exascale Software Challenges in Molecular Dynamics Simulations with GROMACS*.; Springer International Publishing: pp 3-27. doi: 10.1007/978-3-319-15976-8 1.

[61] S. Pronk, S. Pall, R. Schulz, P. Larsson, P. Bjelkmar, R. Apostolov, M.R. Shirts, J. C. Smith, P.M. Kasson, D. van der Spoel, B. Hess, E. Lindahl, *GROMACS 4.5: a high-throughput and highly parallel open source molecular simulation toolkit*, Bioinform. 29 (7) (2013) 845–854, https://doi.org/10.1093/bioinformatics/btt055.

[62] D. Van Der Spoel, E. Lindahl, B. Hess, G. Groenhof, A.E. Mark, H.J. Berendsen, *GROMACS: fast, flexible, and free*, J. Comput. Chem. 26 (16) (2005) 1701–1718, https://doi.org/10.1002/jcc.20291.

[63] C. Oostenbrink, T.A. Soares, N.F. van der Vegt, W.F. van Gunsteren, *Validation of the 53A6 GROMOS force field*, Eur. Biophys. J. 34 (4) (2005) 273–284, https://doi.org/10.1007/s00249-004-0448-6.

[64] Berendsen, H. J. C.; Postma, J. P. M.; van Gunsteren, W. F.; Hermans, J. (1981) *Interaction Models for Water in Relation to Protein Hydration*. In Intermolecular Forces: Proceedings of the Fourteenth Jerusalem Symposium on Quantum Chemistry and Biochemistry Held in Jerusalem, Israel, April 13–16, 1981, Pullman, B. Ed.; Springer Netherlands; pp 331-342. doi: 10.1007/978-94-015-7658-1 21.

[65] A. Nezabi, J. Kalayan, S. Al-Rawashdeh, M.A. Ghattas, R.A. Bryce, *Molecular dynamics simulations as a guide for modulating small molecular aggregation*, J. Comput.-Aided Mol. Design 38 (2024) 11, https://doi.org/10.1007/s10822-024-00557-1.

[66] D.M. van Aalten, R. Bywater, J.B. Findlay, M. Hendlich, R.W. Hooft, G. Vriend, *PRODRG, a program for generating molecular topologies and unique molecular descriptors from coordinates of small molecules*, J. Comput. Aided. Mol. Des. 10 (3) (1996) 255–262, https://doi.org/10.1007/BF00355047.

[67] E. Zuriaga, L. Lomba, F.M. Royo, C. Lafuente, B. Giner, *Aggregation behaviour of betablocker drugs in aqueous media*, New J. Chem. 38 (2014) 4141–4148, https://doi.org/10.1039/C4NJ00112E.

[68] K. Uwai, M. Tani, Y. Ohtake, S. Abe, A. Maruko, T. Chiba, Y. Hamaya, Y. Ohkubo, M. Takeshita, *Photodegradation products of propranolol: the structures and pharmacological studies*, Life Sci. 78 (4) (2005) 357–365, https://doi.org/10.1016/j.lfs.2005.04.033.

[69] G.D. Miles, L. Shedlovsky, *Minima in Surface Tension–Concentration Curves of Solutions of Sodium Alcohol Sulfates*, J. Phys. Chem. 48 (1) (2002) 57–62, https://doi.org/10.1021/j150433a007.

[70] E. Blanco, P.V. Verdes, J.M. Ruso, G. Prieto, F. Sarmiento, *Interactions in binary mixed systems involving betablockers with different lipophilicity as a function of temperature and mixed ratios*, Colloids Surf., A 334 (1–3) (2009) 116–123, https://doi.org/10.1016/j.colsurfa.2008.10.012.

[71] G. Du, Y. Li, S. Ma, R. Wang, B. Li, F. Guo, W. Zhu, Y. Li, *Efficient Determination of the Enantiomeric Purity and Absolute Configuration of Flavanones by Using (S)-3,3′-Dibromo-1,1′-bi-2-naphthol as a Chiral Solvating Agent*, J. Nat. Prod. 78 (12) (2015) 2968–2974, https://doi.org/10.1021/acs.jnatprod.5b00690.

[72] N.J. Heaton, P. Bello, B. Herradón, A. del Campo, J. Jiménez-Barbero, *NMR Study of Intramolecular Interactions between Aromatic Groups: van der Waals, Charge-Transfer, or Quadrupolar Interactions?* J. Am. Chem. Soc. 120 (37) (1998) 9632–9645, https://doi.org/10.1021/ja980528s.

[73] T.S. Sorensen, *On the non-equivalence of isopropyl CH3 nuclear magnetic resonance signals*, Can. J. Chem. 45 (1976), https://doi.org/10.1139/v67-256.

[74] D.M. Pisklak, M. Zielinska-Pisklak, L. Szeleszczuk, I. Wawer, *13-C cross-polarization magic-angle spinning nuclear magnetic resonance analysis of the solid drug forms with low concentration of an active ingredient-propranolol case*, J. Pharm. Biomed. Anal. 93 (2014) 68–72, https://doi.org/10.1016/j.jpba.2013.06.031.

[75] Thordarson, P. (2010) *Determining association constants from titration experiments in.*

[76] *supramolecular chemistry*. Chem. Soc. Rev., **40**, 1305–1323. doi: 10.1039/c0cs00062k.

[77] L.K.S. von Krbek, C.A. Schalley, P. Thordarson, *Assessing cooperativity in supramolecular systems*, Chem. Soc. Rev. 46 (9) (2017) 2622–2637, https://doi.org/10.1039/c7cs00063d.

[78] Bovey, F. A.; Mirau, P. A. (1996) *The solution characterization of polymers*. In NMR of Polymers, Bovey, F. A., Mirau, P. A. Eds.; Academic Press; pp 155-241. doi: 10.1016/B978-012119765-0/50003-2.

[79] A.A. Bredikhin, Z.A. Bredikhina, A.T. Gubaidullin, D.B. Krivolapov, I.A. Litvinov, *Rational approach to a conglomerate-forming propranolol derivative: pointed modifications of the crystal structure*, Mendeleev Commun. 14 (6) (2004) 268–270, https://doi.org/10.1070/MC2004v014n06ABEH002037.

[80] M.H. Hatzopoulos, J. Eastoe, P.J. Dowding, S.E. Rogers, R. Heenan, R. Dyer, *Are hydrotropes distinct from surfactants*, Langmuir 27 (20) (2011) 12346–12353, https://doi.org/10.1021/la2025846.

[81] C. Efthymiou, L. Magnus Bergström, J.N. Pedersen, J.S. Pedersen, P. Hansson, *Self-assembling properties of ionisable amphiphilic drugs in aqueous solution*, J. Colloid Interf. Sci. 600 (2021) 701–710, https://doi.org/10.1016/j.jcis.2021.05.049.

[82] V. Perez-Villar, M.E. Vazquez-Iglesias, A. de Geyer, *Small angle neutron scattering studies of chlorpromazine micelles in aqueous solutions*, J. Phys. Chem. 97 (1993) 5149–5154, https://doi.org/10.1021/j100121a050.

[83] N.A. Seifert, A.S. Hazrah, W. Jager, *The 1-Naphthol Dimer and Its Surprising Preference for pi-pi Stacking over Hydrogen Bonding*, J. Phys. Chem. Lett. 10 (11) (2019) 2836–2841, https://doi.org/10.1021/acs.jpclett.9b00646.

[84] M.W. Schaeffer, W. Kim, P.M. Maxton, J. Romascan, P.M. Felker, *Raman spectroscopy of naphthalene clusters. Evidence for a symmetrical trimer and an unsymmetrical tetramer*, Chem. Phys. Lett. 242 (6) (1995) 632–638, https://doi.org/10.1016/0009-2614(95)00835-r.

[85] W. Kim, M.W. Schaeffer, S. Lee, J.S. Chung, P.M. Felker, *Intermolecular vibrations of naphthalene trimer by ionization-detected stimulated Raman spectroscopy*, J. Chem. Phys. 110 (23) (1999) 11264–11276, https://doi.org/10.1063/1.479067.

[86] S.J. Perkins, D.W. Wright, H. Zhang, E.H. Brookes, J. Chen, T.C. Irving, S. Krueger, D.J. Barlow, K.J. Edler, D.J. Scott, N.J. Terrill, S.M. King, P.D. Butler, J.E. Curtis, *Atomistic modelling of scattering data in the Collaborative Computational Project for Small Angle Scattering (CCP-SAS)*, J. Appl. Crystallogr. 49 (Pt 6) (2016) 1861–1875, https://doi.org/10.1107/S160057671601517X.

[87] M.C. Watson, J.E. Curtis, *Rapid and accurate calculation of small-angle scattering profiles using the golden ratio*, J. Appl. Crystallogr. 46 (4) (2013) 1171–1177, https://doi.org/10.1107/s002188981301666x.

[88] H. Bertagnolli, T. Engelhardt, P. Chieux, *Study of Dipolar Interaction in Liquid Pyridine by X-Ray and Neutron Diffraction*, Ber. Bunsenges. Phys. Chem. 90 (6) (2010) 512–520, https://doi.org/10.1002/bbpc.19860900604.

[89] P.E. Mason, G.W. Neilson, C.E. Dempsey, D.L. Price, M.L. Saboungi, J.W. Brady, *Observation of pyridine aggregation in aqueous solution using neutron scattering experiments and MD simulations*, J. Phys. Chem., B 114 (16) (2010) 5412–5419, https://doi.org/10.1021/jp9097827.

[90] M. Misawa, T. Fukunaga, *Structure of liquid benzene and naphthalene studied by pulsed neutron total scattering*, J. Chem. Phys. 93 (5) (1990) 3495–3502, https://doi.org/10.1063/1.458831.

[91] T.F. Headen, P.L. Cullen, R. Patel, A. Taylor, N.T. Skipper, *The structures of liquid pyridine and naphthalene: the effects of heteroatoms and core size on aromatic interactions*, Phys. Chem. Chem. Phys. 20 (2018) 2704, https://doi.org/10.1039/C7CP06689A.

[92] D. Polenske, H. Lorenz, A. Seidel-Morgenstern, *The binary phase diagram of propranolol hydrochloride and crystallization-based enantioseparation*, J. Pharm. Sci. 99 (4) (2010) 1762–1773, https://doi.org/10.1002/jps.21943.

[93] M. Kuhnert-Brandstätter, R. Völlenklee, *Thermoanalytische und IR-spektroskopische Untersuchungen an polymorphen Arzneistoffen: Acemetacin, Piroxicam, Propranololhydrochlorid und Urapidil*, Fresenius z. Anal. Chem. 322 (2) (1985) 164–169, https://doi.org/10.1007/bf00517654.

[94] Y. Barrans, M. Cotrait, J. Dangoumau, *Conformations cristallines d'adrénolytiques β-bloquants: propranolol et alprénolol*, Acta Cryst., B 29 (6) (1973) 1264–1272, https://doi.org/10.1107/s056774087300436x.

[95] H.L. Ammon, D.B. Howe, W.D. Erhardt, A. Balsamo, B. Macchia, F. Macchia, W. E. Keefe, *The crystal structures of dichloroisoproterenol, propranolol and propranolol hydrochloride*, Acta Cryst., B 33 (1) (1977) 21–29, https://doi.org/10.1107/s0567740877002544.

[96] S.H. Neau, M.K. Shinwari, E.W. Hellmuth, *Melting point phase diagrams of free base and hydrochloride salts of bevantolol, pindolol and propranolol*, Int. J. Pharm. 99 (2–3) (1993) 303–310, https://doi.org/10.1016/0378-5173(93)90373-n.

[97] X. Wang, X.J. Wang, C.B. Ching, *Solubility, metastable zone width, and racemic characterization of propranolol hydrochloride*, Chirality 14 (4) (2002) 318–324, https://doi.org/10.1002/chir.10049.

[98] D. Attwood, S.P. Agarwal, *The surface activity and self-association of some β-adrenoceptor blocking agents in aqueous solution*, J. Pharm. Pharmacol. 31 (1979) 392–395, https://doi.org/10.1111/j.2042-7158.1979.tb13530.x.

[99] N. Hassan, J. Maldonado-Valderrama, A.P. Gunning, V.J. Morris, J.M. Ruso, *Investigating the effect of an arterial hypertension drug on the structural properties of plasma protein*, Colloids Surf. B Biointerfaces 87 (2011) 489–497, https://doi.org/10.1016/j.colsurfb.2011.06.015.

[100] J.M. Ruso, A. González-Pérez, G. Prieto, F. Sarmiento, *A volumetric study of two related amphiphilic beta-blockers as a function of temperature and electrolyte concentration*, Colloids Surf. B Biointerfaces 33 (2004) 165–175, https://doi.org/10.1016/j.colsurfb.2003.10.002.

[101] M. Kozlowska, P. Rodziewicz, T. Utesch, M.A. Mroginski, A. Kaczmarek-Kedziera, *Solvation of diclofenac in water from atomistic molecular dynamics simulations -*

interplay between solute-solute and solute-solvent interactions, Phys. Chem. Chem. Phys. 20 (2018) 8629–8639, https://doi.org/10.1039/c7cp08468d.

[102] D. Attwood, *The mode of association of amphiphilic drugs in aqueous solution*, Adv. Colloid Interf. Sci. 55 (1995) 271–303, https://doi.org/10.1016/0001-8686(94)00228-5.

[103] D. Attwood, V. Mosquera, J.L. Lopez-Fontan, M. Garcia, F. Sarmiento, *Self-Association of Phenothiazine Drugs: Influence of the Counterion on the Mode of Association*, J. Colloid Interf. Sci. 184 (1996) 658–662, https://doi.org/10.1006/jcis.1996.0663.

[104] D. Attwood, P.H. Elworthy, M.J. Lawrence, *Association characteristics of synthetic non-ionic surfactants in aqueous solution*, J. Chem. Soc. Faraday Trans. I 82 (1986) 1903–1910, https://doi.org/10.1039/F19868201903.

[105] D. Attwood, P. Fletcher, *Total intensity and quasi-elastic light scattering studies on the association of amphiphilic drugs in aqueous electrolyte solutions*, J. Colloid Interf. Sci. 115 (1987) 104–109, https://doi.org/10.1016/0021-9797(87)90013-0.

[106] J.J. Irwin, D. Duan, H. Torosyan, A.K. Doak, K.T. Ziebart, T. Sterling, G. Tumanian, B.K. Shoichet, *An aggregation advisor for ligand discovery*, J. Med. Chem. 58 (1) (2015) 7076–7087, https://doi.org/10.1021/acs.jmedchem.5b01105.

[107] O. Roche, P. Schneider, J. Zuegge, W. Guba, M. Kansy, A. Alanine, K. Bleicher, F. Danel, E.M. Gutknecht, M. Rogers-Evans, W. Neidhart, H. Stalder, M. Dillon, E. Sjogren, N. Fotouhi, P. Gillespie, R. Goodnow, W. Harris, P. Jones, M. Taniguchi, S. Tsujii, W. von Der Saal, G. Zimmermann, G. Schneider, *Development of a Virtual Screening Method for Identification of "Frequent Hitters" in Compound Libraries*, J. Med. Chem. 45 (2002) 137–142, https://doi.org/10.1021/jm010934d.

[108] B.Y. Feng, A. Simeonov, A. Jadhav, K. Babaoglu, J. Inglese, B.K. Shoichet, C. P. Austin, *A high-throughput screen for aggregation-based inhibition in a large compound library*, J. Med. Chem. 50 (2007) 2385–2390, https://doi.org/10.1021/jm061317y.